Title: Coordination between ECM and cell-cell adhesion regulates the development of islet aggregation, architecture, and functional maturation

Wilma Tixi[1, 5], Maricela Maldonado[1, 5], Ya-Ting Chang[1, 5], Nazia Parveen[1], Amy Chiu[1], Ryan Hart[2], Shihao Wang[3], Wu Jih Hsu[3], Janel L. Kopp[3], Mark O. Huising[2,4], Sangeeta Dhawan[1], and Hung-Ping Shih[1, *]

[1] Department of Translational Research and Cellular Therapeutics, Arthur Riggs Diabetes and Metabolic Research Institute, Beckman Research Institute, City of Hope, Duarte, CA, USA

[2] Department of Neurobiology, Physiology and Behavior, College of Biological Sciences, University of California, Davis, Davis, CA, USA

[3] Department of Cellular and Physiological Sciences, Life Sciences Institute, University of British Columbia, Vancouver, British Columbia, Canada

[4] Department of Physiology and Membrane Biology, School of Medicine, University of California, Davis, Davis, CA, USA

[5] These authors contributed equally to this work

[*]Corresponding author: hshih@coh.org

HIGHLIGHTS

- Islet vascularization and aggregation are regulated via ECM-Itgb1 signaling
- ECM-Itgb1 signaling negatively controls islet aggregation via regulation of cell-cell adhesion during development
- Cell-cell adhesion negatively regulates the interaction of endocrine cell-vasculature in islets
- Differential cell adhesion regulates the establishment of islet architecture
- Endocrine functional maturation depends on islet aggregation regulated by the coordination of ECM-Itgb1 signaling and cell-cell adhesion

SUMMARY

Pancreatic islets are 3-dimensional aggregates consisting of unique cellular composition, cell-to-cell contacts, and interactions with blood vessels. Islet cell aggregation is essential for proper endocrine cell function; however, it remains unclear how developing islets establish aggregation. By combining genetic animal models, imaging tools, and gene expression profiling, we demonstrate that the formation of islet aggregates is regulated by extracellular matrix signaling and cell-cell adhesion. Islet endocrine progenitor cell-specific inactivation of extracellular matrix receptor Integrin β1 disrupted vasculature but promoted cell-cell adhesion and the formation of larger islets, while ablation of cell-cell adhesion molecule α-Catenin promoted vasculature formation yet compromised islet clustering. Simultaneous removal of Integrin β1 and α-Catenin abrogates islet aggregation. These mutants exhibit disruption of the endocrine cell maturation process, demonstrating that establishment of islet aggregates is essential for functional maturation. Our study provides new insights into understanding the fundamental self-organizing mechanism for islet aggregation, architecture, and functional maturation.

INTRODUCTION

To control various physiological responses, groups of endocrine cells cluster together with vasculature, mesenchymal cells, and neuronal cells to form a highly organized "mini-organ" in the pancreatic epithelium: the islet of Langerhans. The islet endocrine cells emerge from a domain of multipotent progenitors in the embryonic pancreatic epithelium. Initially, the multipotent pancreatic progenitors resolve into a pre-acinar domain, and a bipotential endocrine/ductal progenitor domain of the developing pancreas (Larsen and Grapin-Botton, 2017; Romer and Sussel, 2015; Shih et al., 2013). Endocrine cell progenitors are specified by the expression of the pro-endocrine gene *Neurogenin 3* (*Ngn3*) (Gu et al., 2002). Following endocrine cell specification, the Ngn3^{+} precursors undergo delamination (Bechard et al., 2016; Gouzi et al., 2011; Rosenberg et al., 2010). Delaminated endocrine precursors remain associated with the ducts as they migrate and join other endocrine cells and aggregate into immature islets (Sharon et al., 2019a). These immature islets form long interconnected cords along the ductal epithelium. Later the islet cords change morphology and undergo fission to form distinct spherical islets (Jo et al., 2011; Seymour et al., 2004; Sznurkowska et al., 2020). Throughout the differentiation and morphological changes, endocrine cells are intimately associated with the vasculature, which facilitates functional control of hormone release (Reinert et al., 2014). To coordinate the hormone release of endocrine cells within each islet, autocrine and paracrine interactions, as well as direct cell contacts are required (Campbell and Newgard, 2021). These interactions are established by the aggregation process during development (Adams and Blum, 2022). Defects in the aggregation processes may lead to defects in endocrine cell development, and eventually, islet dysfunction. Supporting this notion, human pluripotent stem cell-derived β-cells acquire more functional maturity *in vitro* if clustered together (Cottle et al., 2021; Nair et al., 2019). However, the mechanism by which this process is regulated *in vivo* has largely remained elusive.

Self-organization of a group of cells into a higher-order, multicellular functional unit relies on an array of cell interactions regulated by cell-cell adhesions (Fagotto, 2014). For example, a calcium-dependent adhesion molecule, Neural Cell Adhesion Molecule (N-CAM), has been shown to be critical for murine endocrine cells to cluster (Esni et al., 1999). In rodents, islets form a stereotypical core-mantle architecture in which the Insulin (Ins) secreting β-cells are located mainly in the central core, with Glucagon (Gcg) secreting α-cells and Somatostatin (Sst) secreting δ-cells localizing in the periphery to form a mantle (Adams and Blum, 2022; Arrojo e Drigo et al., 2015; Kim et al., 2009). In culture, dissociated rat endocrine cells can self-organize into the core–mantle architecture, suggesting that the islet structure is established by factors intrinsic to

endocrine cells (Halban et al., 1987). N-CAM deleted mice showed abnormal islet architecture, with α-cells spread throughout the islet core and abnormal assembly of adherens junction proteins N- and E-cadherin (Ncad and Ecad) (Esni et al., 1999). In addition, ectopic expression of a dominant negative Ecad in mouse β-cells interferes with their clustering and islet formation (Dahl et al., 1996); and loss of *Ecad* results in abnormal blood glucose homeostasis (Wakae-Takada et al., 2013). Intracellularly, adherens junctions are stabilized by β-Catenin (*Ctnnb1*) and α-Catenin (*Ctnna1*) (Jamora and Fuchs, 2002). The function of *Ctnnb1* has been extensively studied in the developing pancreas (Elghazi et al., 2012; Murtaugh et al., 2005; Rulifson et al., 2007) and in hPSC-derived β-cells, because of its role in cell proliferation via Wnt signaling (Sharon et al., 2019b); yet genetic studies show that *Ctnnb1* is not essential for islet clustering and architecture (Elghazi et al., 2012; Murtaugh et al., 2005). In the developing pancreas, inactivation of *Ctnna1* results in defects in endocrine progenitor differentiation due to an expansion of pancreatic ductal progenitors (Jimenez-Caliani et al., 2017). Whether the process of islet clustering and architecture requires *Ctnna1* is unknown.

The regulation of cell-cell adhesions is often coupled with cell-extracellular matrix (ECM) interaction and Integrin signaling (Mui et al., 2016; Weber et al., 2011). Upon ECM binding, Integrins activate signal transduction pathways and regulate 1) cytoskeleton dynamics, 2) cell movement, 3) cell differentiation, and 4) functional maturation of epithelial cells, the vasculature and neurons (Barros et al., 2011; Li et al., 2008; Scheppke et al., 2012). For example, during angiogenesis, ECM receptor Integrin β1 (Itgb1) is required to control the localization of cell-cell adhesion molecule VE-cadherin and maintain cell–cell junction integrity (Yamamoto et al., 2015). In salivary glands and early embryonic pancreas, Integrin β1-mediated ECM adhesions regulate Ecad to control cell clustering and regulate budding epithelial branching (Shih et al., 2016; Wang et al., 2021; Wang et al., 2017). Whether islet morphogenesis also requires ECM-Integrin signaling remains to be investigated.

In the present study, we examine how loss of *Itgb1* and *Ctnna1* in Ngn3-expressing endocrine progenitors affects islet morphogenesis. We showed that *Itgb1* and *Ctnna1* have collaborative roles during islet aggregation: ECM-Itgb1 signaling modulates islet aggregation by negatively regulating cell-cell adhesions; and α-Catenin promotes endocrine cell clustering and modulates vascularization during islet development. We also provided evidence that the islet architecture is regulated by differential adhesion in endocrine subtypes.

RESULTS

The morphogenesis and functional maturation of islet endocrine cells depend on ECM-Itgb1 signaling during development

To investigate the process of islet aggregation, confocal 3D image of embryonic day 15.5 (E15.5) pancreas stained for blood vessel maker PECAM, ductal marker Spp1, and endocrine cell marker Chromogranin was analyzed. At E15.5 the endocrine cells had just begun aggregating, and the vascular and ductal networks were already highly similar (Figure S1A). This close relation between the ducts and blood vessels at the stage prior to islet aggregation suggests that blood vessels could readily interact and provide instructive cues to regulate endocrine progenitor aggregation into islets. Blood vessels in islets produce ECM-rich basal membrane to support and organize endocrine cells (Lammert et al., 2003; Roscioni et al., 2016). We thus hypothesized that ECM signaling provided by the vasculature plays a key role in the initiation steps of islet aggregation. Supporting this notion, published work using single-cell gene expression profiling shown that the ECM-Itgb1 signaling gene ontology (GO) categories are most significantly enriched in the Ngn3^{+} endocrine progenitors (Bastidas-Ponce et al., 2019). Immunofluorescence (IF) analysis validated that both the Ngn3^{+} endocrine progenitors and their progenies (eYFP^{+} cells in *Ngn3-Cre; Rosa26-eYFP* pancreas) expressed Itgb1 (Figure 1A). To investigate the role of Itgb1 during endocrine cell aggregation, we used the *Ngn3-Cre* allele to recombine the *Itgb1-flox* alleles in endocrine progenitors (*Ngn3-Cre*; *Itgb1*$^{f/f}$; hereafter *Itgb1*$^{\Delta Endo/\Delta Endo}$). Expression of Itgb1 was almost entirely absent throughout the islet endocrine cells in comparison to control littermates by 6 weeks old (Figure 1B,1C). We first examined whether inactivation of ECM-Itgb1 signaling affected vascular interaction. Electron microscope ultrastructure analysis revealed tight attachment in basal membranes between vascular and endocrine cells in control islets (Figure S1B). In contrast, with the *Itgb1*$^{\Delta Endo/\Delta Endo}$ islets, the endocrine cells were detached from the basal membranes of vasculature (Figure S1C, red arrows). Despite the vascular defects with Itgb1 loss, all four endocrine cell subtypes, α-, β-, δ-, and Ppy- (pancreatic polypeptide) cells, were present at similar proportions in control and *Itgb1*$^{\Delta Endo/\Delta Endo}$ islets (Figure 1D,1E;S1D-S1G). In addition, the expression of β-cell lineage markers Nkx6.1 and Pdx1 were present in the Ins^{+} cells of control and *Itgb1*$^{\Delta Endo/\Delta Endo}$ islets (Figure 1F,1G). Although the populations of endocrine cell lineages were unaffected by the loss of *Itgb1*, morphometrical analysis revealed drastic morphological changes. In control islets, β-cells were organized in a central core and surrounded by α- and δ- cells in the periphery (Figure 1D). Conversely, in *Itgb1*$^{\Delta Endo/\Delta Endo}$ mice, several individual islets appeared to agglomerate, resulting in larger islet sizes and aberrant distribution of α- and δ- cells in the central

core (Figure 1E,1G; S1H). Thus, the inactivation of Itgb1 has a profound impact on islet morphogenesis, but not endocrine cell fate choice.

We next investigated whether the expression of genes associated with islet function were affected by the loss of *Itgb1*. Islets from 6 weeks old control and *Itgb1*$^{\Delta Endo/\Delta Endo}$ mice were isolated and subjected to RNA-seq and differential gene expression analysis. A comparison of gene-expression profiles between *Itgb1*$^{\Delta Endo/\Delta Endo}$ and control islets revealed 417 differentially expressed genes (DEGs) with false discovery rate (FDR) < 0.05 and fold change (FC)>2 (Table S2), of which 332 were up-regulated and 85 were down-regulated. Gene-set enrichment analysis (GSEA) of DEGs between control and *Itgb1*$^{\Delta Endo/\Delta Endo}$ islets showed up-regulation of pathways associated with hypoxia, epithelial mesenchymal transition, glycolysis, and inflammatory response. The down-regulated genes were associated with spermatogenesis, pancreas β-cells, and E2F targets (Figure 1H). GO analysis of DEGs in the pancreas β-cells category further revealed that functional maturation genes for β-cells (e.g., *Slc2a2* (Glut2, *Ucn3*, and *Mafa*) and for α-cells (e.g., *Arx*, *Mafb*, and *Etv1*), were drastically down-regulated in the *Itgb1*$^{\Delta Endo/\Delta Endo}$ islets (Figure 1I, Group 1). IF analysis also validated the reduced expression of Mafa, Ucn3, and Glut2 in β-cells of *Itgb1*$^{\Delta Endo/\Delta endo}$ islets (Figure S1I-L). Furthermore, several “disallowed” genes for β-cells, including *Ldha1*, *Aldh1a3*, and *Hk1* (Lemaire et al., 2016), were significantly up-regulated in the *Itgb1*$^{\Delta Endo/\Delta Endo}$ islets (Figure 1I, Group 2). This suggests that the endocrine cells present in *Itgb1*$^{\Delta Endo/\Delta Endo}$ islets might have defects in functional maturation. Consistent with this, *Itgb1*$^{\Delta Endo/\Delta Endo}$ mice were glucose-intolerant by 6 weeks of age (Figure 1J). The glycemia regulation worsened when mice were older than 6 months (Figure 1K). Furthermore, genes involved in the hypoxia response pathway were up-regulated in the *Itgb1*$^{\Delta Endo/\Delta Endo}$ islets compared to controls (Figure S1M). IF analysis showed that the vasculature were largely excluded from the *Itgb1*$^{\Delta Endo/\Delta Endo}$ islets by 2-3 months old (Figure S1N-S1P), suggesting that the failure of vascular interactions leads to hypoxia responses. Together, these observations indicate that ECM-integrin interactions are critical for islet vascularization, morphogenesis, and the functional maturation of endocrine cells.

ECM signaling controls islet aggregation by regulating cell-cell adhesion during development

Consistent with the observations on tissue sections, the islets isolated from *Itgb1*$^{\Delta Endo/\Delta Endo}$ mice spontaneously clumped into huge aggregates in culture (Figure 2A-2C); however, the total islet area was not affected in the *Itgb1*$^{\Delta Endo/\Delta Endo}$ mice (Figure 2D). The size differences were mainly due to changes in the large islets (>10^3 pixels^2, Figure 2E. Thus, the enlarged islet size is likely due to a morphological alteration independent of total endocrine cell expansion. Furthermore,

normally islets were near the ducts but separate in control pancreata (Figure 2F,2H); however, islets in the *Itgb1*$^{\Delta Endo/\Delta Endo}$ pancreata contained more ductal cells (Figure 2G,2H). Segmentation analysis on 3D WMIF images further revealed that the majority of *Itgb1*-deleted endocrine cell aggregates had a greater tendency to cluster within the ductal cords during development at E15.5 (Figure 2I,2J; green color represented zero distance to ducts; Movie S1). This suggests defects both in endocrine cell migration and premature islet aggregation. To further validate this, we performed live-imaging analysis on pancreas explants from E16.5 *Ngn3-Cre; R26mT/mG* (control) and *Ngn3-Cre; R26mT/mG; Itgb1*$^{f/f}$ (*Itgb1*$^{\Delta Endo/\Delta Endo}$) mice to follow the movement and aggregation of Ngn3-progeny cells (mGFP^{+}) in explant cultures for up to 3 days (Figure S2A,S2B; Movie S2,S3). In contrast to controls, in which the endocrine progenitor cells migrate and aggregate outside of ductal cords, the mGFP^{+} cells in *Itgb1*$^{\Delta Endo/\Delta Endo}$ explants readily aggregate before moving away from the cords (Figure S2A,S2B white arrows). These data suggest that Itgb1 signaling regulates the migration and aggregation of cells in the endocrine lineage during developmental stages. To test whether Itgb1 signaling also maintains islet cell aggregation after β-cell maturation and islet formation has already taken place, we crossed *Ucn3-Cre* with *Itgb1*$^{f/f}$ mice to inactivate Itgb1 only in mature β-cells (hereafter *Itgb1*$^{\Delta Mature\beta/\Delta Mature\beta}$). In *Itgb1*$^{\Delta Mature\beta/\Delta Mature\beta}$ mice, we observed the exclusion of vasculature from islets similar to *Itgb1*$^{\Delta Endo/\Delta Endo}$ mice, but the islet size was similar to controls (Figure S2C,S2D). Thus, islet cell aggregation is controlled by Itgb1 signaling specifically during pancreatic development.

In addition to the differences in islet size, RNA-seq analysis identified misregulation of genes controlling gap junction, tight junction, and cytoskeleton dynamics in Itgb1-deficient islets (Figure S2E-S2G). As cell junctions link actin cytoskeleton to maintain cell shape, the inactivation of *Itgb1* in endocrine cells could also lead to an alteration in cell shape. Indeed, endocrine cells of *Itgb1*$^{\Delta Endo/\Delta Endo}$ islets exhibited a shape change from a flattened truncated tetrahedra to rigid hexagon and showed cell compaction (Figure S2H,S2I). These findings suggested that Itgb1 may regulate islet aggregation by controlling cell-cell adhesions. We analyzed Airyscan super-resolution images of Ecad IF on endocrine cells in *Ngn3-Cre; R26mT/mG; Itgb1*$^{f/f}$ islets at P7, as islet aggregation is complete by the neonatal stages (Sznurkowska et al., 2020). The Airyscan images provide sufficient resolution to show adherens junctions between cells by visualizing Ecad^{+} clusters ((Gonschior et al., 2020); white dots in Figure 1K,1L) The lineage-traced endocrine cells (mGFP^{+}) in control islets displayed low amounts of Ecad^{+} clusters (Figure 2K). However, the amount of Ecad^{+} clusters was drastically increased in mutant islets (Figure 2L), suggesting that Itgb1 signaling negatively regulates cell adhesion in developing islets. To further test whether the increased cell adhesiveness is responsible for increased islet size when Itgb1 signaling is

disrupted, we performed an *in vitro* cell aggregation assay. Live mGFP$^+$ endocrine cells from neonatal (P2-P4) *Ngn3-Cre; R26mT/mG; Itgb1$^{+/f}$* or *Ngn3-Cre; R26mT/mG; Itgb1$^{f/f}$* pancreata were completely dissociated, then collected by FACS. 3000 mGFP$^+$ cells were allowed to aggregate in wells of a 96-well plate that were coated with bovine serum albumin (no ECM) or Matrigel and fibronectin (+ECM) (Figure 2M). Within 2 hours of cell seeding, the control mGFP$^+$ endocrine cells rapidly aggregated in wells with no ECM coating but formed no aggregates in the ECM-coated wells (Figure 2N-2P). Within the same amount of time, the mutant mGFP$^+$ endocrine cells clustered into larger aggregates in wells without ECM coating and maintained aggregation in the ECM-coated wells (Figure 2N,2Q,2R). After 48 hours, the mGFP$^+$ cells isolated from both the controls and mutants progressively clustered into larger aggregates in wells without ECM coating (Figure S2J-S2L,S2N). In contrast, in the ECM-coated wells, only the mutant mGFP$^+$ cells clustered, while control mGFP$^+$ cells remained unaggregated (Figure S2K,S2M,S2O). Together, these findings demonstrated that ECM-Itgb1 signaling negatively regulates islet aggregation. Mechanistically, these Itgb1-deficient endocrine cells could increase their adhesion to each other by promoting cell-cell adhesion, resulting in larger islet aggregates.

α-Catenin promotes endocrine cell aggregation and regulates vascularization during islet development

Our findings revealed that Itgb1 plays an essential role in islet development by modulating endocrine cell-cell adhesion. We sought to study how cell-cell adhesion regulates islet formation. To do this we conditionally inactivated α-Catenin (Ctnna1), the essential hub protein linking Ecad-mediated adherens junctions to cytoskeleton (Jamora and Fuchs, 2002), in endocrine progenitors by generating *Ngn3-Cre*; *Ctnna1$^{f/f}$* mice (hereafter *Ctnna1$^{\Delta Endo/\Delta Endo}$*). To determine whether *Ctnna1* deletion affects islet development, Chromogranin A (ChrA) staining on pancreas sections from 8 weeks old mice were imaged and total relative islet area measured. Compared to their wild-type littermates, total islet area in *Ctnna1$^{\Delta Endo/\Delta Endo}$* mice was unchanged, but there was a significant reduction in average islet size (Figure 3A-3D). The proportion of larger islets was significantly reduced, while the proportion of small islets was increased (Figure S3A), suggesting that *Ctnna1* is required for proper islet aggregation, but not for the development of total islet cell mass. In *Ctnna1$^{\Delta Endo/\Delta Endo}$* islets, the expression of Ecad was abrogated and endocrine cells were hypertrophic, suggesting the loss of adherens junctions and low cell adhesion in Ctnna1-deficint endocrine cells (Figure 3E,3F). As Ctnna1 links cell-cell adhesion complexes to the actin cytoskeleton and regulates the dynamics of filamentous actin (F-actin), *Ctnna1$^{\Delta Endo/\Delta Endo}$* islets showed the abnormal organization of F-actin fibers, such that

the fibers were no longer aligned parallel to lateral sides of endocrine cells as in control islets (Figure 3E,3F;S3B,S3C). These findings demonstrated that the loss of Ctnna1 compromised endocrine cell aggregation and perturbs the organization of actin cytoskeleton and cell-cell adhesion.

To investigate how *Ctnna1*-deletion impacts islet development, we compared transcriptional profiling of *Ctnna1*$^{\Delta Endo/\Delta Endo}$ and control islets at 8 weeks. A comparison of gene-expression profiles between *Ctnna1*$^{\Delta Endo/\Delta Endo}$ and control islets revealed significant differences in the expression of 319 genes with FDR < 0.05 and FC>2, of which 245 were up-regulated and 74 were down-regulated (Table S3). Consistent with the role of Ctnna1 in the regulation of cytoskeleton, *Ctnna1*$^{\Delta Endo/\Delta Endo}$ islets exhibited a significant up-regulation for genes associated with cytoskeleton regulation (Figure S3D). Among all GO categories, one of the most up-regulated groups in *Ctnna1*$^{\Delta Endo/\Delta Endo}$ islets is genes associated with ECM signaling and blood vessel interactions (Figure 3G). These include Metalloproteases, Vascular Adhesion, Collagens, Integrins, Laminins, Glycoproteins and Thrombospondins (Figure 3G). These findings suggested that *Ctnna1*$^{\Delta Endo/\Delta Endo}$ islets have augmented ECM signaling and blood vessel interaction. IF for blood vessels confirmed an increased islet vasculature density in *Ctnna1*$^{\Delta Endo/\Delta Endo}$ islets at 8 weeks (Figure 3H-3J). The increased islet vasculature density was observed as early as P14 (Figure 3K-3L;S3E-S3F). Thus, the augmented blood vessel interaction may be the result of developmental processes during islet aggregation. These findings demonstrated that the inactivation of *Ctnna1* in endocrine progenitor cells led to a decrease of endocrine cell-cell adhesion and an increase in blood vessel interaction. Together these findings show that the balance between cell-cell adhesion and blood vessel interaction mediates islet cell aggregation during development (Figure S3G).

Inactivation of Ctnna1 in differentiating endocrine cells affects the assembly and maintenance of non-β endocrine cells in islets

The comparison of gene-expression profiles between *Ctnna1*$^{\Delta Endo/\Delta Endo}$ and control islets also revealed significant misregulation in genes critical for endocrine cell functions. The expression of *Slc27a2*, *Tmsb15b1*, and *Etv1*, genes required for glycemic control and insulin secretion, was down-regulated in *Ctnna1*$^{\Delta Endo/\Delta Endo}$ islets (Figure 4A, Group 1), while the expression of *Hk1, Ldha, Aldh1a1,* and *Cxcl14*, genes known to be “disallowed” in mature functional β-cells (Lemaire et al., 2016), was up-regulated (Figure 4A, Group 2). Thus, β-cell function may be negatively affected in *Ctnna1*$^{\Delta Endo/\Delta Endo}$ mice. Supporting this notion, glucose tolerance tests performed at 8 weeks

revealed mild glucose intolerance in *Ctnna1*$^{\Delta Endo/\Delta Endo}$ mice (Figure 4B); and the glucose intolerance phenotype was more pronounced at one year of age (Figure 4C). Surprisingly, besides the suggested functional defects in β-cells, genes for non-β endocrine cell lineages, including α-cell genes *Gcg, MafB, Arx, Peg10,* and *Etv1,* and the δ-cell gene *Sst*, were significantly down-regulated in *Ctnna1*$^{\Delta Endo/\Delta Endo}$ islets (Figure 4A), suggesting the requirement of *Ctnna1* for the presence of non-β endocrine cells in islets. Indeed, *Ctnna1*$^{\Delta Endo/\Delta Endo}$ islets did not show a reduced area of β-cells, as β-cells were still organized loosely in the core of islets (Figure 4D-4F). However, there was a severe reduction of α-cell and δ-cell populations in the *Ctnna1*-deleted islets (Figure 4E,4G;S4A-S4C). To determine whether the loss of non-β endocrine cells was the result of differentiation defects during development, we examined the population of α- and β-cells in *Ctnna1*$^{\Delta Endo/\Delta Endo}$ islets at P0 and P7. At these ages, the islets of *Ctnna1*$^{\Delta Endo/\Delta Endo}$ mice exhibited normal endocrine cell mass and Gcg^{+} α-cell area (Figure 4H,4I;S4D-S4G), demonstrating that the loss of α-cells was not due to differentiation defects prior to these early stages. However, the detachment of α-cell from the mantle of *Ctnna1*$^{\Delta Endo/\Delta Endo}$ islets was observed by P7. At this time point, normally α-cells had formed tight interaction with other endocrine cells in control islets (Figure S4E,S4H), but *Ctnna1*-deficint α-cells detached from other cell types (Figure S4G,S4I). To investigate whether the cell detachment promotes cell death and results in α-cell loss, TUNEL analysis on P7 *Ctnna1*$^{\Delta Endo/\Delta Endo}$ islets were conducted to analyze cell apoptosis. Compared to control, *Ctnna1*$^{\Delta Endo/\Delta Endo}$ islets display 3 times more TUNEL^{+} apoptotic α-cells (Figure 4J-4L), indicating that *Ctnna1* is required for α-cell survival. Thus, the loss of the α-cells in *Ctnna1*$^{\Delta Endo/\Delta Endo}$ islets during adulthood therefore is not due to endocrine cell differentiation defects; instead, a drastic increase in apoptosis explains the loss of α-cells in the *Ctnna1*-deleted islets.

Differential adhesion in endocrine cells controls the formation of islet architectures

Since the reduction of cell-cell adhesion caused distinctive outcomes in different endocrine cell subtypes, we hypothesized that the endocrine cells in the mantle or core of islets may have different adhesiveness. We re-analyzed publicly available gene expression profiles (DiGruccio et al., 2016) to examine the expression of key cell-adhesion molecules *E-cadherin*, *N-cadherin*, *α-Catenin*, and *β-Catenin* between the subtypes of endocrine cells. These adhesion genes were expressed at the highest level in β-cells, while their expression was comparatively lower in endocrine cells located in the mantle of islets (α-cells and δ-cells, Figure S5A). These observations suggested the adhesive properties of different endocrine cell subtypes may differ. According to the differential adhesion hypothesis (DAH), a population of cells with different

adhesive properties will tend to spontaneously sort themselves to maximize adhesive bonding (Foty and Steinberg, 2005). Stronger adhesion between β-cells may lead to them to be bundled into islet cores, while weaker adhesion between non-β-cells results in them being dispersed into islet mantles. To test the DAH, we crossed *Gcg-iCre* and *Ins1-Cre* lines to *Ctnna1-flox* mice and traced the *Ctnna1*-deleted cells with the lineage tracer *Rosa26-mT/mG* (*Gcg-iCre; Ctnna1*$^{f/f}$; *Rosa26-mT/mG,* and *Ins1-Cre*; *Ctnna1*$^{f/f}$; *Rosa26-mT/mG*, hereafter *Ctnna1*$^{\Delta\alpha/\Delta\alpha}$ and *Ctnna1*$^{\Delta\beta/\Delta\beta}$, respectively). Based on the DAH, we predict that Ctnna1-expressing α-cells will be merged into the core of *Ctnna1*$^{\Delta\beta/\Delta\beta}$ islets due to weaker adhesion in the *Ctnna1*-deleted β-cells. The *Rosa26-mT/mG* lineage-tracing allele faithfully reported the *Gcg-iCre* and *Ins1-Cre* cell lineages (Figure 5A,5G). Supporting the notion that α-cells have low adhesive properties, the assembly of F-actin was loosely bundled between α-cells (Figure S5B,S5C). In contrast, β-cells exhibited strong F-actin assembly with well-organized and rigid rosette structures; however, inactivation of *Ctnna1* in β-cells drastically reduced the formation of F-actin (Figure S5D,S5E), suggesting a decrease of cell adhesion assemblies in β-cells of *Ctnna1*$^{\Delta\beta/\Delta\beta}$ islets. The mGFP^{+} α-cells of *Ctnna1*$^{\Delta\alpha/+}$ mice are mostly located on the mantle of islets (Figure 5A,5E), and the mGFP^{+} β-cells of *Ctnna1*$^{\Delta\beta/+}$ mice are mostly located on the core of islets (Figure 5C,5G). As DAH predicted, β-cell-specific *Ctnna1*-deletion led to α-cells entering the core of islets (Figure 5D). These observations support the idea that differential adhesion between endocrine subtypes is a contributing factor for establishing the islet architecture during development; and the weaker cell adhesion in the peripheral islet layers leads to the specific loss of these cell types in *Ctnna1*$^{\Delta Endo/\Delta Endo}$ islets (Figure 5I).

Coordination of ECM and cell-cell adhesion regulates islet vascularization, architecture, and functional maturation

Our studies showed that the cell-ECM and cell-cell adhesion regulate islet development coordinately to balance the endocrine cell and blood vessel interactions; when one aspect of these adhesions is perturbed, islet endocrine cells may compensate with another interaction to maintain islet aggregation (Figure S3G). We next asked whether islet clustering relies solely on these two adhesions. To test this, we simultaneously removed cell-ECM and cell-cell adhesion in all endocrine progenitor cells by generating *Ngn3-Cre; Ctnna1*$^{f/f}$*; Itgb1*$^{f/f}$ (hereafter *Ctnna1; Itgb1*$^{\Delta Endo/\Delta Endo}$) double knockout (DKO) mice. We compared control, *Ctnna1*$^{\Delta Endo/\Delta Endo}$, *Itgb1*$^{\Delta Endo/\Delta Endo}$, and DKO islets at P7 to examine their morphology. Consistent with observations at the later ages, the P7 *Ctnna1*$^{\Delta Endo/\Delta Endo}$ islets displayed loosely aggregated endocrine cells, increased vascularization (Figure 6A,6B), reduced F-actin assemblies, and more active-Itgb1^{+}

endothelial cells in the loosened islet aggregates (Figure S6A,S6B). Conversely, P7 *Itgb1*$^{\Delta Endo/\Delta Endo}$ islets clumped together (Figure 6C), with strong F-actin assemblies and less active-Itgb1^{+} endothelial cells in the tightly aggregated islets (Figure S6C). However, the aggregation of endocrine cells was completely abrogated in the DKO mice (Figure 6D). These DKO endocrine cells became suspended single cells scattered throughout the entire pancreatic epithelium, displaying rounded cell morphology (Figure 6D). The DKO endocrine cells were larger and displayed weak F-actin assemblies (Figure S6D). Despite the drastic changes in endocrine cell aggregation and morphology, the endocrine cell subtypes were still present in the P7 DKO islets (Figure 6D and data not shown), suggesting that the differentiation of endocrine subtype is independent of the islet aggregation process. To determine whether the failure in the islet aggregation affected endocrine cell maturation, IF for β-cell maturation markers was performed. In P7 mice, Ucn3 and Glut2 were robustly expressed in the cytosol and cell surface of control β-cells (Figure 6E,6I). Deletion of *Ctnna1* or *Itgb1* in endocrine progenitor cells led to reduced expression of Ucn3 and Glut2 in β-cells (Figure 6F,6G,6J,6K). This observation was consistent with the gene profiling analysis from 8 weeks old mice, reiterating the notion that the ECM and cell adhesion control β-cell maturation. Finally, the DKO islets displayed a severe loss of these β-cell maturation markers in P7 β-cells (Figure 6H,6L). The reduced expression of β-cell maturation markers Ucn3 and Glut2 persisted in 8 weeks old DKO mice (Figure 6M-6P); and these mice are severely glucose intolerant (Figure S6E), indicating that the functional maturation of β-cells depends on islet aggregation. Together, our findings support a model whereby islet morphogenesis, vasculature interaction, endocrine cell aggregation, and the β-cell maturation process are coordinately regulated by cell-ECM and cell-cell adhesion during development (Figure S6F).

DISCUSSION

Our study reveals the combinatorial roles of cell-ECM and cell-cell adhesion in regulating the aggregation of endocrine cells into islets. Mechanistically, islet cell aggregation depends on endocrine cell-cell adhesion, which is negatively regulated by cell-ECM adhesion through vascular interaction. These two adhesion properties are reciprocally regulated: lowering cell-ECM adhesion promotes endocrine cell-cell adhesion; and, conversely, lowering cell-cell adhesion promotes cell-ECM adhesion. Importantly, the aggregation and functional maturation processes of endocrine cells are affected by the loss of either adhesion property and further affected by the loss of both.

As both *Itgb1*$^{\Delta Endo/\Delta Endo}$ and *Itgb1*$^{\Delta Mature\beta/\Delta Mature\beta}$ mice show reduced vascularization, the involvement of ECM signaling in vascular interactions is critical in both embryonic endocrine cells and mature β-cells. This concurs with the study using *MIP-Cre* to generate *Itgb1*-knockout mice, which showed reduced islet vascularization (Win et al., 2020). The involvement of Itgb1 signaling in organ vascularization appears to be a universal requirement: as shown in pituitary endocrine epithelial cells and kidney cells, Itgb1-inactivation leads to vasculature loss (Mohamed et al., 2020; Scully et al., 2016). The expression of *Vegfa*, an essential growth factor for islet vasculature, is not affected in *Itgb1*$^{\Delta Endo/\Delta Endo}$ islets (Table S2). Thus, the reduced vascularization in Itgb1-deficient islets may not be due to vasculature growth defects. Downstream of Integrin signaling, integrin-linked kinase (ILK) is activated upon Integrin-ECM binding to regulate actin organization, cell migration, and other cellular processes (Hannigan et al., 2005). Genetic deletion of ILK in developing pancreas leads to the failure of ILK-inactivated endocrine cells to adhere to the basement membrane, and drastic reduction of intra-islet blood vessel density (Kragl et al., 2016). This study further showed that cortical actomyosin contraction was significantly increased, thus increasing cortex tension in both the ILK-deleted islets, as well as in Itgb1-inactivated cultured β-cells. Our analyses showed aberrant organization of F-actin fibers and compaction of individual endocrine cells, as well as dysregulated cytoskeleton genes in Itgb1-deleted islets. Thus, it is likely that both the *Itgb1*$^{\Delta Endo/\Delta Endo}$ and *Itgb1*$^{\Delta Mature\beta/\Delta Mature\beta}$ islets fail to interact with vasculature resulting in the same alteration of the actomyosin regulation seen in ILK-deleted islet cells. As well, *Ctnna1*$^{\Delta Endo/\Delta Endo}$ model shows increased islet vascularization without affecting the expression of *Vegfa* (Table S3). We posit that weakened adhesion between endocrine cells in *Ctnna1*$^{\Delta Endo/\Delta Endo}$ islets may allow greater penetration of vasculature through islet clusters, leading to augmented islet vascularization. Supporting this notion, salivary gland patterning allows vessel penetration via an epithelial "cleft" created by weakened cell-cell adhesion (Kwon et al., 2017). Interestingly, the initial steps of cleft formation requires ECM-Itgb1 signaling (Sakai et al., 2003);

conversely, reducing cell-cell adhesion promotes cell-ECM adhesion during budding morphogenesis (Wang et al., 2021). Thus, our proposed model, in which ECM signaling in concert with cell-cell adhesion controls islet aggregation, reflects a fundamental mechanism of organ morphogenesis.

During the induction of the proendocrine cell program, expression of Ngn3 promotes the activation of ECM signaling. This is thought to regulate the delamination and migration of proendocrine cells from the ductal progenitor cords (Rosenberg et al., 2010). Supporting this notion, inactivation of ECM signaling in endocrine progenitor cells led to reduced migration distance as these endocrine cells remained intermingled with ducts post-differentiation. ECM signaling activation to regulate endocrine cell migration appears to be required only in early developmental stages, as the *Itgb1*$^{\Delta Mature\beta/\Delta Mature\beta}$ islets do not show migration defects. This is also supported by other studies using *Ins-Cre* or *RIP-Cre* to ablate *Itgb1* after endocrine progenitors have already differentiated into insulin-producing cells, as those studies do not report observable migration defects (Diaferia et al., 2013; Win et al., 2020). This suggests that ECM-Integrin signaling are critical for endocrine cell migration, and that the time window for endocrine cell initiation is small. A previous study showed that, during this window, islet cell radial migration is controlled by semaphorin signaling (Pauerstein et al., 2017). Semaphorin-induced actin remodeling is linked to alterations in the cell's anchorage to the ECM (Alto and Terman, 2017). Thus, the chemoattractant system where semaphorin signaling occurs may involve the activation of Itgb1 signaling to control islet progenitor cell migration toward the periphery, and away from the ducts. Whether the migration of endocrine progenitors toward the periphery affects their function, remains to be tested.

Despite the endocrine subtype ratios being different in human versus rodent islets, the precise differences in the stereotypical architectures in the two species have been debated. Studies using different imaging analysis have yielded different conclusions (Dybala et al., 2020). In mice, it is proposed that spatiotemporal collinearity leads to the typical core-mantle architecture of the spherical islet in which α-cells, the first to develop, form the peninsular outer layer, and β-cells subsequently form beneath them (Sharon et al., 2019a). Our current study has not directly tested this hypothesis, yet our observation suggests that differential cell adhesion is critical for developing this structure. Our data support a model in which randomly allocated α- and β-cells are specified and sorted into the final islet architecture based on differential adhesion. It remains to be tested whether the differential cell adhesion also involves in the development of islet architectures in human. In addition, studies have shown that the Roundabout (Robo)/Slit signaling axis plays a role in determining islet stereotypical architecture. The secreted ligand, Slit, is often associated with ECM, and binds to Robo receptors to control various cellular responses via

cytoplasmic kinases and regulation of actin and microtubule cytoskeleton (Jiang et al., 2022; Tong et al., 2019). Mice lacking *Robo1* and *Robo2* in all endocrine cells, or selectively in β cells, show complete loss of endocrine cell type sorting in the islets (Adams et al., 2021; Adams et al., 2018; Gilbert et al., 2020). Interestingly, Robo1/2 double knockout islets exhibit adhesion defects and are prone to dissociate upon isolation (Adams et al., 2018), similar to the *Ctnna1*$^{\Delta Endo/\Delta Endo}$ islets. Similar observations have been shown in stem cell sorting and cancer cell migration; binding of Slit to Robo receptors leads to the modulation of Ncad- or Ecad-mediated cell adhesion (Stine et al., 2014; Tong et al., 2019). We speculate that Robo/Slit signaling regulates endocrine cell type sorting in islets by controlling cell adhesive properties to establish the islet architecture.

Limitation of the study

The dynamic nature of islet aggregation and endocrine subtype sorting would require more in depth live-imaging analysis. Obtaining 3D cellular information in developing islets would provide insights into these dynamic and complex phenomena, and further our understanding of the process of islet development and morphogenesis. We anticipate that using pancreas slice cultures (Panzer et al., 2020) for to develop an imaging platform to monitor the development live neonatal islets would provide a framework for understanding how islet develop, and offer novel ways to harness this understanding in the search for clinical alternatives to treat diabetes.

AUTHOR CONTRIBUTIONS

W.T., M.M., Y.T.C, and H.P.S. conceived the project, designed the experiments, and analyzed the data. W.T., M.M., Y.T.C performed all analysis of mouse genetic models and live-imaging experiments. Y.T.C performed in vitro islet cell aggregation assay. A.C. assembled figures and graphical summaries. N.P. and S.D. analyzed the RNA-seq data and generated heatmaps. R.H and M.H. analyzed *Ucn3-Cre* mice model and prepared gene expression genome viewer plots. S.W., W.J.H., and J.L.K. conceived *Ctnna1*^{flox} mouse breeding and experiments. W.T., M.M., and H.P.S. wrote the manuscript.

ACKNOWLEDMENTS

We thank Dr. Maike Sander for sharing the anti-Ngn3 antiserum and Dr. Rupangi Vasavada for sharing the *Ins-Cre* mouse strain. We acknowledge the support of City of Hope Core Facilities; Michael Nelson and Dr. Brain Armstrong from the Microscopy Core, Dr. Zhuo Li from the Electron Microscopy Core, Drs. Xiwei Wu and Min-Hsuan Chen from the Integrative Genomics Core, Dr. Patrick Fueger from Comprehensive Metabolic Phenotyping Core at City of Hope. Wanek Family Foundation to Cure Type 1 Diabetes and NIH/NIDDK 1R01DK119590 to H.P.S., NIH/NIDDK 1R01DK120523, Human Islet Research Network (HIRN) New investigator Award (subaward via UC4DK104162), and a grant from the Wanek Family Foundation to Cure Type 1 Diabetes to S.D., NSERC Discovery Grant (RGPIN-2016-04276), CIHR New Investigator Award, and MSFHR Scholar Award to J.L.K, NIH/NIDDK 1R01DK110276 to M.O.H., JDRF postdoctoral fellowship 3-PDF-2019-742-A-N to M.M. The California Institute for Regenerative Medicine (CIRM) Train Grant EDUC4-12772 to W.T.

FIGURES

FIGURE 1

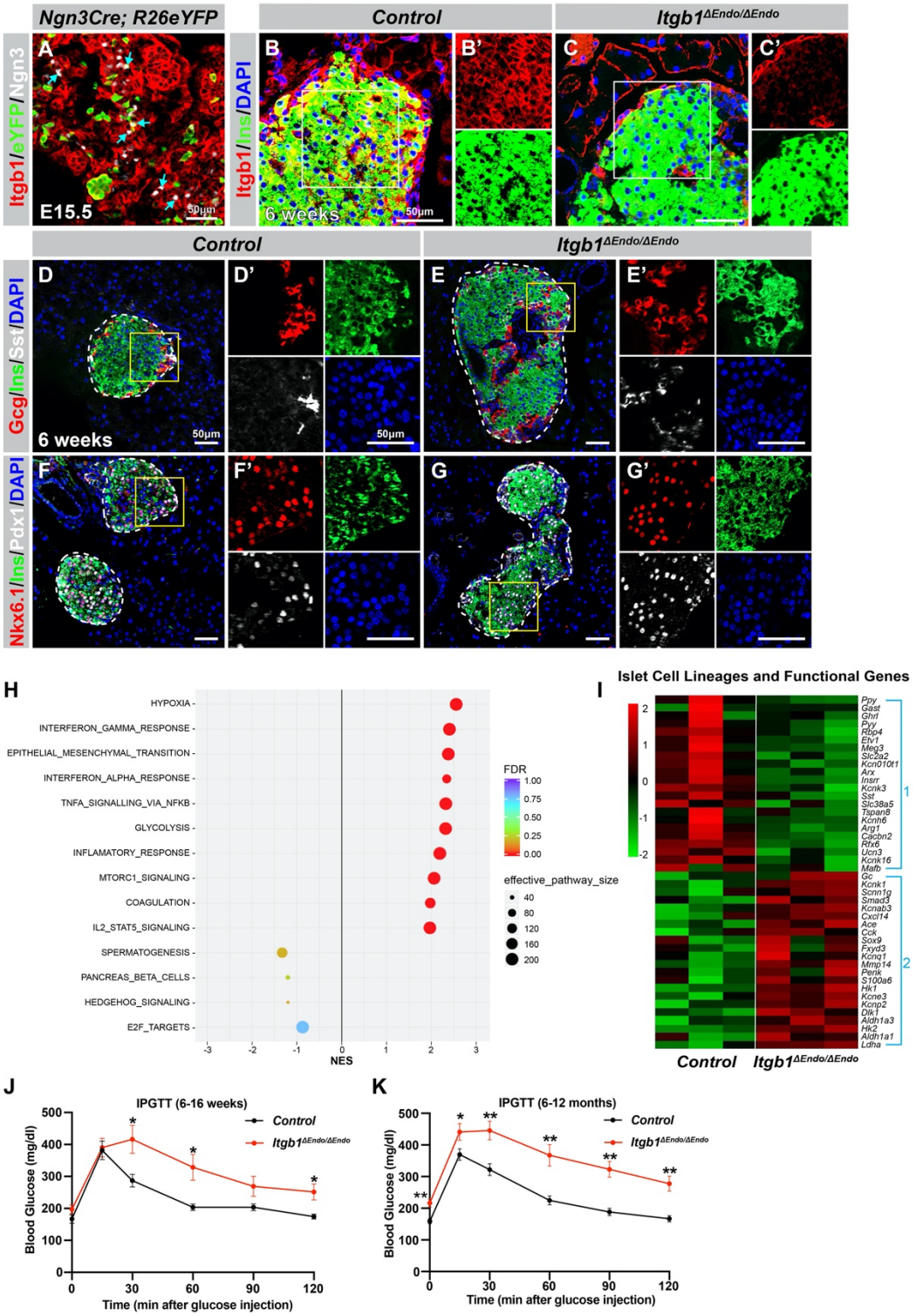

Figure 1. ECM-Itgb1 signaling in endocrine progenitors is required for normal islet morphology and function.

(A) Immunofluorescence staining for Itgb1 and Ngn3 in *Ngn3-Cre; Rosa26eYFP* reporter mice pancreas section at E15.5. Arrows show $Ngn3^{+}$ cells and lineage traced endocrine cells expressing Itgb1. (B-C) Immunofluorescence staining for Itgb1, Ins, and DAPI on pancreas sections showing robust *Itgb1*-deletion in an $Itgb1^{\Delta Endo/\Delta Endo}$ islet at 6 weeks old. Similar size islets from control and $Itgb1^{\Delta Endo/\Delta Endo}$ pancreas sections were selected for a clear image comparison. Fields demarcated by white boxes in B-C are shown with individual color channels in B'-C' side panels. (D-G) Immunofluorescence staining for Gcg, Ins, Sst, Nkx6.1, Pdx1, and DAPI on pancreas sections of (D,F) control and (E,G) $Itgb1^{\Delta Endo/\Delta Endo}$ mice at 6 weeks old. Individual islets are outlined by dotted lines. Fields demarcated by yellow boxes in D-G are shown at higher magnification in D'-G' side panels. (H) Gene-set enrichment analysis of the differentially expressed genes showing top enriched pathways for control versus $Itgb1^{\Delta Endo/\Delta Endo}$ islets. Gene sample sizes and FDRs are indicated by the size and color of the dots. (I) Heatmap showing down-regulation (Group 1) and up-regulation (Group 2) of functional maturation genes in $Itgb1^{\Delta Endo/\Delta Endo}$ islets compared to controls. (J-K) Intraperitoneal glucose tolerance test on (J) 6 to 16 weeks old and (K) 6 to 12 months old control and $Itgb1^{\Delta Endo/\Delta Endo}$ mice.

Ngn3, Neurogenin 3; Gcg, Glucagon; Ins, Insulin; DAPI, 4',6-diamidino-2-phenylindole; Sst, Somatostatin; IPGTT, intraperitoneal glucose tolerance test; FDR, false discovery rate; E15.5, embryonic day 15.5

Data are shown as mean ± SEM. * $p < 0.05$ and ** $p < 0.01$.

SUPPLEMENTARY FIGURE 1: RELATED TO FIGURE 1

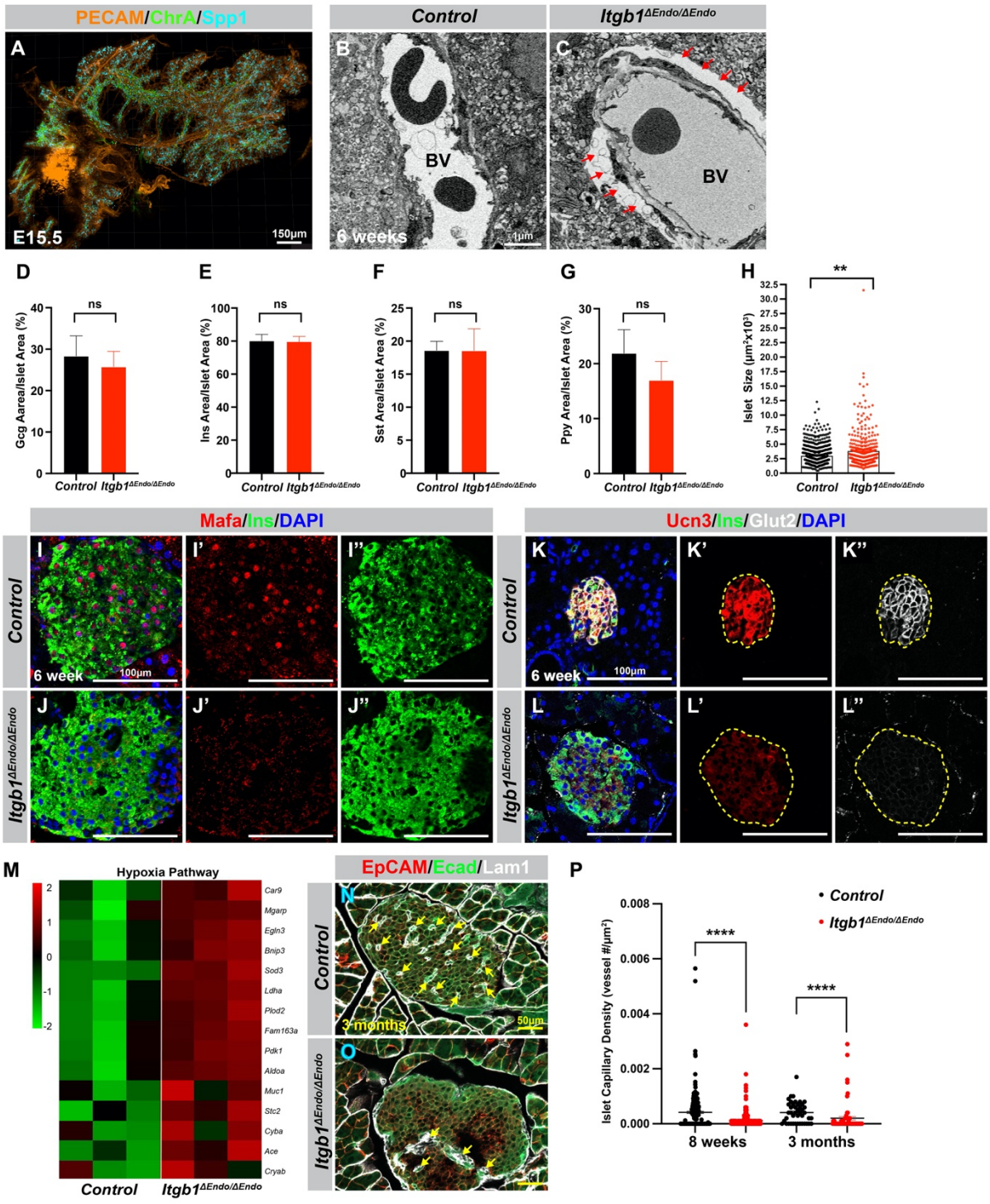

Figure S1. Deletion of *Itgb1* in endocrine progenitors results in abnormal interactions with blood vessels and decreased expression of functional maturation markers within islets. Related to Figure 1.

(A) Whole mount immunofluorescence staining for PECAM, ChrA, and Spp1 in a wild-type pancreas at E15.5. (B-C) Transmission electron microscope images showing blood vessels in 6 weeks old islets. Deletion of *Itgb1* disrupts the attachment of endocrine cells to blood vessels (red arrows) in *Itgb1*$^{\Delta Endo/\Delta Endo}$ islets. (D-G) Quantification of the percentage of (D) Gcg^{+}, (E) Ins^{+}, (F) Sst^{+}, and (G) Ppy^{+} cells relative to measured islet area of 6 weeks old control and *Itgb1*$^{\Delta Endo/\Delta Endo}$ pancreas sections. (H) Quantification of overall islet sizes based on ChrA staining of 6 weeks old control and *Itgb1*$^{\Delta Endo/\Delta Endo}$ pancreas sections. (I-L) Immunofluorescence staining for Mafa, Ins, Ucn3, Glut2 and DAPI on 6 weeks old (I, K) control and (J, L) *Itgb1*$^{\Delta Endo/\Delta Endo}$ pancreas sections. Individual islets are outlined by dotted yellow lines in (K',L'). (M) Heatmap showing hypoxia pathway genes are up-regulated in *Itgb1*$^{\Delta Endo/\Delta Endo}$ islets. (N-O) Immunofluorescence staining for EpCAM, Ecad, and Lam1 on 3 months old pancreas sections showing reduced islet vasculature indicated by Lam1^{+} cells (yellow arrows). (P) Quantification of islet blood vessel density in control or *Itgb1*$^{\Delta Endo/\Delta Endo}$ islet area at 8 weeks and 3 months old.

PECAM, Platelet endothelial cell adhesion molecule-1; ChrA, Chromogranin A; Spp1, Secreted Phosphoprotein 1; Gcg, Glucagon; Ins, Insulin; Sst, Somatostatin; Ppy, Pancreatic Polypeptide; Urocortin 3, Ucn3; Ecad, E-cadherin; BV, blood vessels; Epithelial cellular adhesion molecule, EpCAM; Lam1, Laminin1; DAPI, 4',6-diamidino-2-phenylindole; E15.5, embryonic day 15.5

Data are shown as mean ± SEM. ** $p < 0.01$ and **** $p < 0.0001$.

FIGURE 2

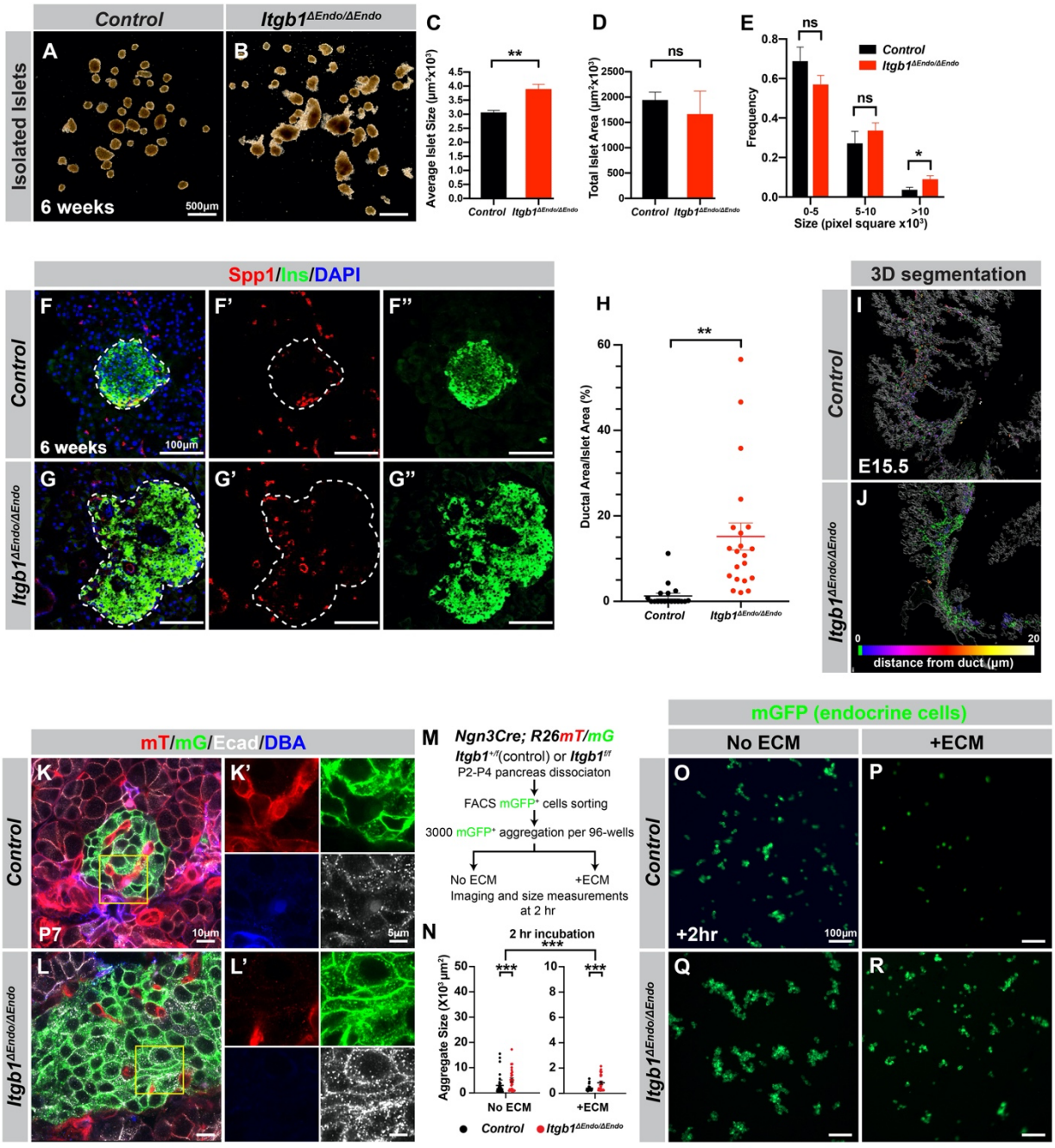
Control
Itgb1ΔEndo/ΔEndo
Isolated Islets
A
B
6 weeks
500µm
C
Average Islet Size (µm²x10³)
**
Control
Itgb1ΔEndo/ΔEndo
D
Total Islet Area (µm²x10³)
ns
E
Frequency
ns
*
0-5
5-10
>10
Size (pixel square x10³)
Spp1/Ins/DAPI
F
F'
F''
G
G'
G''
100µm
H
Ductal Area/Islet Area (%)
**
3D segmentation
I
E15.5
J
0
20
distance from duct (µm)
mT/mG/Ecad/DBA
K
K'
P7
10µm
5µm
L
L'
M
Ngn3Cre; R26mT/mG
Itgb1+/f(control) or Itgb1f/f
P2-P4 pancreas dissociaton
FACS mGFP+ cells sorting
3000 mGFP+ aggregation per 96-wells
No ECM
+ECM
Imaging and size measurements at 2 hr
N
2 hr incubation
***
Aggregate Size (X10³ µm²)
No ECM
+ECM
mGFP (endocrine cells)
No ECM
+ECM
O
P
Q
R
+2hr
100µm

Figure 2. Itgb1 signaling is required for proper endocrine progenitor aggregation.

(A-B) Brightfield images of isolated islets from control and *Itgb1*$^{\Delta Endo/\Delta Endo}$ mice at 6 weeks old. (C-E) Quantification of (C) average islet size, (D) total islet area, and (E) islet size distribution based on ChrA staining on 6 weeks old control and *Itgb1*$^{\Delta Endo/\Delta Endo}$ pancreas sections. (F-G) Immunofluorescence staining for Spp1, Ins, and DAPI on 6 weeks old control and *Itgb1*$^{\Delta Endo/\Delta Endo}$ pancreas sections. Islets are outlined by white dotted lines. (H) Quantification of the ratio of ductal cell areas within islets based on Spp1 and ChrA staining on 6 weeks old control and *Itgb1*$^{\Delta Endo/\Delta Endo}$ pancreas sections. (I-J) 3D segmentation analysis on whole mount immunofluorescence images of E15.5 control and *Itgb1*$^{\Delta Endo/\Delta Endo}$ pancreata stained for ChrA and Spp1, showing the endocrine cells in *Itgb1*$^{\Delta Endo/\Delta Endo}$ pancreas are mostly retained within ducts. The distance between endocrine cells and ducts is represented by a color scale. (K-L) Airyscan super-resolution image of immunofluorescence staining for Ecad and ductal marker DBA in P7 mT/mG reporter mice showing up-regulation of Ecad in the *Itgb1*$^{\Delta Endo/\Delta Endo}$ pancreas. Dot-like Ecad expression pattern in super-resolution imaging represents adherens junction structures. Fields demarcated by yellow boxes in K-L are shown at higher magnification in K'-L' side panels. (M) Schematic of the experimental design for *in vitro* aggregation assay. (N) Quantification of aggregate size after 2 hours of incubation with or without ECM. (O-R) Fluorescence images of mGFP^{+} endocrine progenitor aggregates after 2 hours of culture. mGFP^{+} control endocrine progenitors clustered (O) without ECM but remained single cells (P) with ECM. Alternatively, *Itgb1*$^{\Delta Endo/\Delta Endo}$ endocrine progenitors clustered (Q) without ECM or (R) with ECM.

ChrA, Chromogranin A; Spp1, Secreted Phosphoprotein 1; Ins, Insulin; DAPI, 4',6-diamidino-2-phenylindole; Ecad, E-cadherin; DBA, Dolichos Biflorus Agglutinin; P7, postnatal day 7; E15.5, embryonic day 15.5

Data are shown as mean ± SEM. * $p < 0.05$, ** $p < 0.01$ and *** $p < 0.001$.

SUPPLEMENTARY FIGURE 2: RELATED TO FIGURE 2

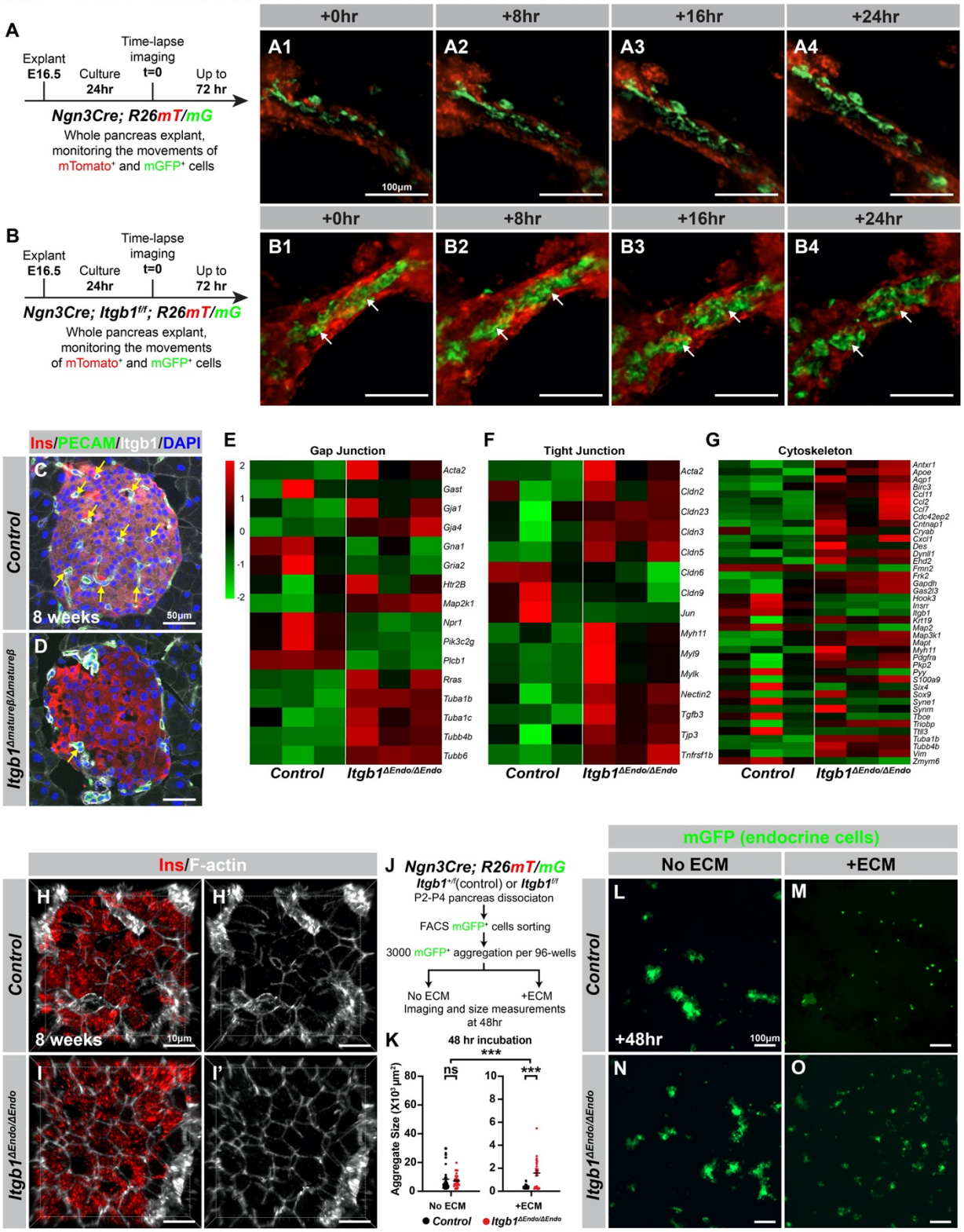

Figure S2. Itgb1 is required for normal islet architecture. Related to Figure 2.

(A-B) Time-lapse confocal microscope imaging of endocrine progenitor cell behaviors in E16.5 embryonic pancreas explants. Live cell imaging time-course of first 24 hours to monitor cell movement in (A1-A4) control and (B1-B4) *Itgb1*$^{\Delta Endo/\Delta Endo}$ pancreas explants. White arrows indicate prematurely clustered islets in *Itgb1*$^{\Delta Endo/\Delta Endo}$ explants. (C-D) Immunofluorescence staining for Ins, PECAM, Itgb1, and DAPI on 8 weeks old (C) control and (D) *Itgb1*$^{\Delta Mature\beta/\Delta Mature\beta}$ pancreas sections. In *Itgb1*$^{\Delta Mature\beta/\Delta Mature\beta}$ islets the presence of Itgb1 and vasculature in the islet is abolished. (E-G) Heatmap showing up-regulation of (E) gap junction, (F) tight junction, and (G) cytoskeleton genes in 8 weeks old *Itgb1*$^{\Delta Endo/\Delta Endo}$ islets. (H-I) Immunofluorescence staining for Ins and F-actin on 8 weeks old control and *Itgb1*$^{\Delta Endo/\Delta Endo}$ pancreas sections. (J) Schematic of experimental design for *in vitro* aggregation assay. (K) Quantification of aggregate size after 48 hours incubation with or without ECM in control and *Itgb1*$^{\Delta Endo/\Delta Endo}$ endocrine progenitors. (L-O) Fluorescence images of mGFP^{+} endocrine progenitor aggregates after 48 hours culture. mGFP^{+} control endocrine progenitors clustered (L) without ECM but remained single cells (M) with ECM after 48 hours. Alternatively, *Itgb1*$^{\Delta Endo/\Delta Endo}$ endocrine progenitors clustered (N) without ECM or (O) with ECM after 48 hours.

Ins, Insulin; PECAM, Platelet endothelial cell adhesion molecule-1; ChrA, Chromogranin A; DAPI, 4',6-diamidino-2-phenylindole; E16.5, embryonic day 16.5

Data are shown as mean ± SEM. *** $p < 0.001$.

FIGURE 3

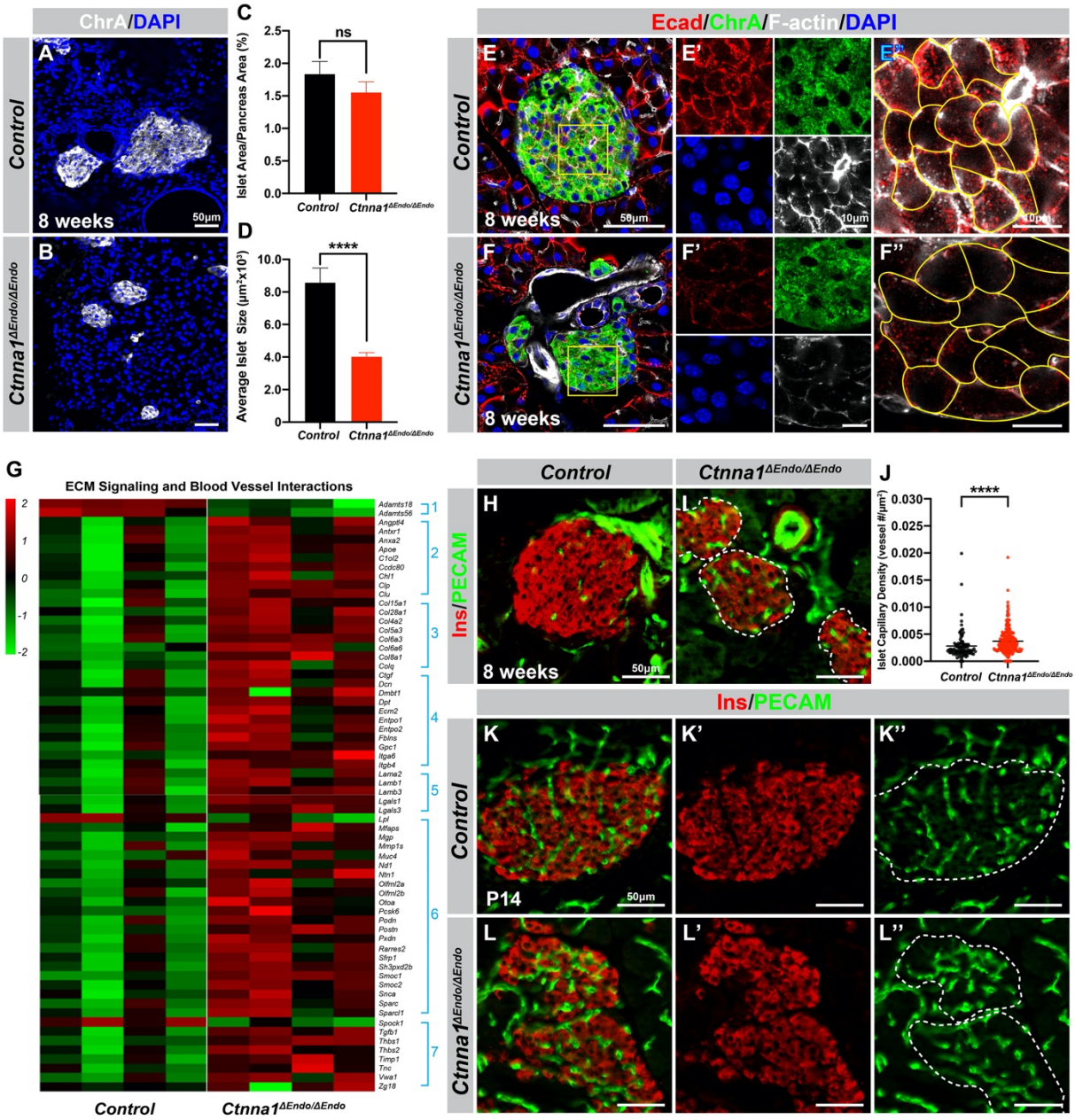
ChrA/DAPI
Control
Ctnna1ΔEndo/ΔEndo
A
B
8 weeks
50µm
C
ns
Islet Area/Pancreas Area (%)
Control
Ctnna1ΔEndo/ΔEndo
D
****
Average Islet Size (µm²x10³)
Ecad/ChrA/F-actin/DAPI
E
E'
E''
F
F'
F''
10µm
G
ECM Signaling and Blood Vessel Interactions
Adamts18
Adamts56
Angptl4
Anbtr1
Anxa2
Apoe
C1ql2
Ccdc80
Chl1
Clp
Clu
Col15a1
Col28a1
Col4a2
Col5a3
Col6a3
Col6a6
Col8a1
Colq
Ctgf
Dcn
Dmbt1
Dpt
Ecm2
Entpo1
Entpo2
Fbln5
Gpc1
Itga6
Itgb4
Lama2
Lamb1
Lamb3
Lgals1
Lgals3
Lpl
Mfaps
Mgp
Mmp1s
Muc4
Nd1
Ntn1
Olfml2a
Olfml2b
Otoa
Pcsk6
Podn
Postn
Pxdn
Rarres2
Sfrp1
Sh3pxd2b
Smoc1
Smoc2
Snca
Sparc
Sparcl1
Spock1
Tgfb1
Thbs1
Thbs2
Timp1
Tnc
Vwa1
Zg18
Control
Ctnna1ΔEndo/ΔEndo
Ins/PECAM
H
I
8 weeks
50µm
J
****
Islet Capillary Density (vessel #/µm²)
K
K'
K''
P14
L
L'
L''

Figure 3. Ctnna1-mediated cell-cell adhesion is required for normal islet morphology and endocrine cell aggregation.

(A-B) Immunofluorescence staining for ChrA and DAPI in 8 weeks old pancreas sections showing smaller islet sizes in *Ctnna1*$^{\Delta Endo/\Delta Endo}$ mice. (C-D) Quantification of (C) the percentage of islet area in pancreas area and (D) average islet size based on ChrA staining on 8 weeks old control and *Ctnna1*$^{\Delta Endo/\Delta Endo}$ pancreas sections. (E-F) Airyscan images of immunofluorescence staining for Ecad, ChrA, F-actin, and DAPI for control and *Ctnna1*$^{\Delta Endo/\Delta Endo}$ pancreas sections. Fields demarcated by yellow boxes are shown at higher magnification with individual color channels in E'-F' middle panels, showing reduced expression of Ecad and F-actin in *Ctnna1*$^{\Delta Endo/\Delta Endo}$ islets. Individual endocrine cell shape is delineated by yellow lines in E"-F", demonstrating the enlarged endocrine cell sizes in the islets of *Ctnna1*$^{\Delta Endo/\Delta Endo}$ mice. (G) Heatmap showing genes for ECM signaling and blood vessel interactions are up-regulated in *Ctnna1*$^{\Delta Endo/\Delta Endo}$ islets at 8 weeks old. Groups 1-7 represent gene ontologies of: 1) Metalloproteases, 2) Vascular Adhesion 3) Collagens, 4) Integrins, 5) Laminins, 6) Glycoproteins and 7) Thrombospondins. (H-I) Immunofluorescence staining of Ins and PECAM on 8 weeks old control and *Ctnna1*$^{\Delta Endo/\Delta Endo}$ pancreas sections. (J) Quantification of islet blood vessel density based on Ins and PECAM staining on 8 weeks old control and *Ctnna1*$^{\Delta Endo/\Delta Endo}$ pancreas sections. (K-L) Immunofluorescence staining of Ins and PECAM on P14 control and *Ctnna1*$^{\Delta Endo/\Delta Endo}$ pancreas sections showing increased vasculature in *Ctnna1*$^{\Delta Endo/\Delta Endo}$ islets. Islet area is outlined by dotted lines.

ChrA, Chromogranin A; DAPI, 4',6-diamidino-2-phenylindole; Ecad, E-cadherin; Ins, Insulin; PECAM, Platelet endothelial cell adhesion molecule-1; P14, postnatal day 14

Data are shown as mean ± SEM. **** $p < 0.0001$.

SUPPLEMENTARY FIGURE 3: RELATED TO FIGURE 3

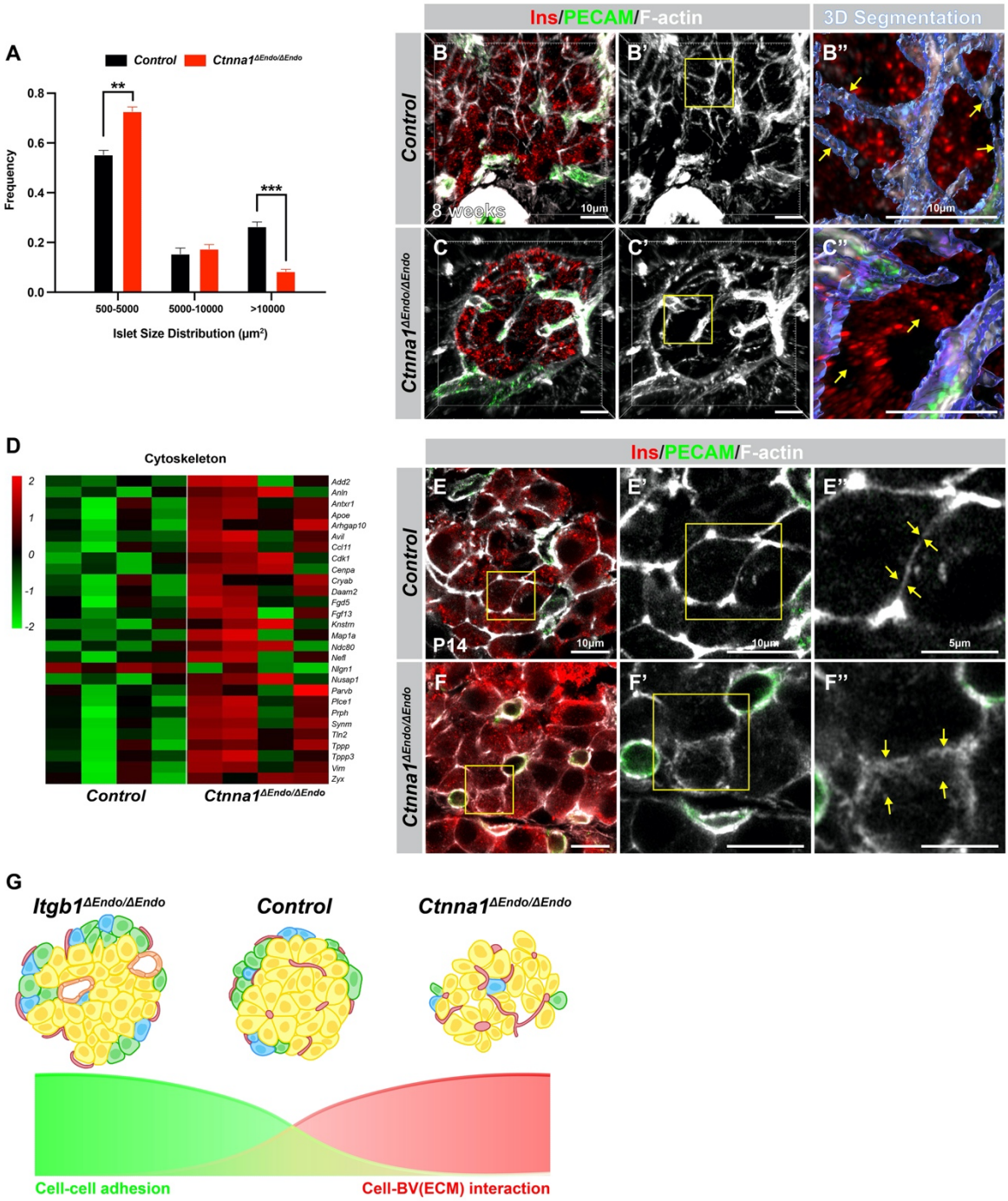

Figure S3. *Ctnna1*-deleted pancreatic islet endocrine cells display cytoskeleton anomalies. Related to Figure 3.

(A) Quantification of islet size distribution based on ChrA staining for 8 weeks old control and *Ctnna1*$^{\Delta Endo/\Delta Endo}$ pancreas sections. (B-C) 3D Airyscan images of immunofluorescence staining for Ins, PECAM and F-actin on 8 weeks old control and *Ctnna1*$^{\Delta Endo/\Delta Endo}$ pancreas sections. Fields demarcated by yellow boxes in B'-C' are shown at higher magnification in B"-C". (B"-C") 3D segmentation of the Airyscan images shows the loss of F-actin between Ins-expressing endocrine cells. (D) Heatmap showing up-regulated cytoskeleton gene expression in 8 weeks old *Ctnna1*$^{\Delta Endo/\Delta Endo}$ islets. (E-F) Airyscan images of immunofluorescence staining for Ins, PECAM, and F-actin in P14 control and *Ctnna1*$^{\Delta Endo/\Delta Endo}$ pancreas sections. Yellow arrows indicate F-actin assemblies. (G) Graphical summary showing cell-cell adhesion and cell-blood vessel (BV) interaction differences observed in *Itgb1*$^{\Delta Endo/\Delta Endo}$ and *Ctnna1*$^{\Delta Endo/\Delta Endo}$ islets.

Ins, Insulin; PECAM, Platelet endothelial cell adhesion molecule-1; P14, postnatal day 14; BV, blood vessels

Data are shown as mean ± SEM. ** $p < 0.01$ and *** $p < 0.001$.

FIGURE 4

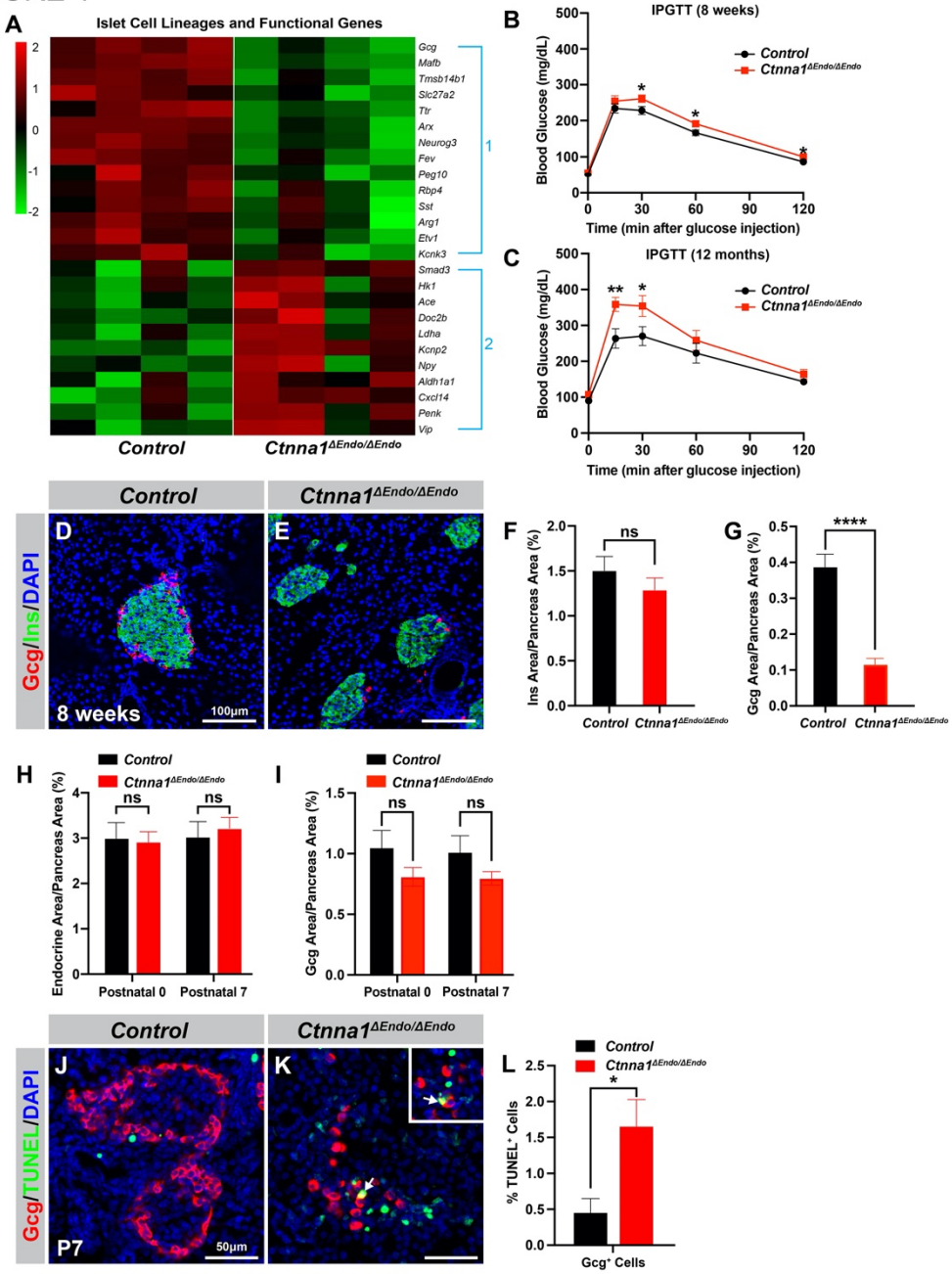
A
Islet Cell Lineages and Functional Genes
Gcg
Mafb
Tmsb14b1
Slc27a2
Ttr
Arx
Neurog3
Fev
Peg10
Rbp4
Sst
Arg1
Etv1
Kcnk3
Smad3
Hk1
Ace
Doc2b
Ldha
Kcnp2
Npy
Aldh1a1
Cxcl14
Penk
Vip
Control
Ctnna1ΔEndo/ΔEndo
B
IPGTT (8 weeks)
Blood Glucose (mg/dL)
Time (min after glucose injection)
C
IPGTT (12 months)
D
E
Gcg/Ins/DAPI
8 weeks
100µm
F
Ins Area/Pancreas Area (%)
ns
G
Gcg Area/Pancreas Area (%)
****
H
Endocrine Area/Pancreas Area (%)
Postnatal 0
Postnatal 7
I
Gcg Area/Pancreas Area (%)
J
K
Gcg/TUNEL/DAPI
P7
50µm
L
% TUNEL+ Cells
Gcg+ Cells

Figure 4. Ctnna1 is required for proper islet functionality and α-cell survival.

(A) Heatmap showing the top up-regulated endocrine cell lineage genes (Group 1) and down-regulated functional genes (Group 2) in 8 weeks old *Ctnna1*$^{\Delta Endo/\Delta Endo}$ islets. (B-C) Intraperitoneal glucose tolerance test of (B) 8 weeks old and (C) 12 months old control and *Ctnna1*$^{\Delta Endo/\Delta Endo}$ mice. (D-E) Immunofluorescence staining for Gcg, Ins, and DAPI on 8 weeks old (D) control and (E) *Ctnna1*$^{\Delta Endo/\Delta Endo}$ pancreas sections showing the reduction of α-cells. (F-G) Quantification of (F) Ins^{+} or (G) Gcg^{+} area relative to total pancreas area in 8 weeks old control and *Ctnna1*$^{\Delta Endo/\Delta Endo}$ pancreas sections. (H) Quantification of endocrine cell area relative to total pancreas area in control and *Ctnna1*$^{\Delta Endo/\Delta Endo}$ pancreas sections at P0 and P7. (I) Quantification of Gcg^{+} area relative to the total pancreas area in control and *Ctnna1*$^{\Delta Endo/\Delta Endo}$ pancreas sections at P0 and P7. (J-K) Immunofluorescence staining for Gcg, TUNEL, and DAPI for P7 control and *Ctnna1*$^{\Delta Endo/\Delta Endo}$ pancreas sections. (L) Quantification of the percentage of TUNEL^{+}/Gcg^{+} co-positive cells relative to total Gcg^{+} cell numbers in P7 control and *Ctnna1*$^{\Delta Endo/\Delta Endo}$ islets.

Gcg, Glucagon; Ins, Insulin; DAPI, 4',6-diamidino-2-phenylindole; IPGTT, intraperitoneal glucose tolerance test; TUNEL, terminal deoxynucleotidyl transferase dUTP nick end labeling; P0, postnatal day 0; P7, postnatal day 7

Data are shown as mean ± SEM. * $p < 0.05$, ** $p < 0.01$.

SUPPLEMENTARY FIGURE 4: RELATED TO FIGURE 4

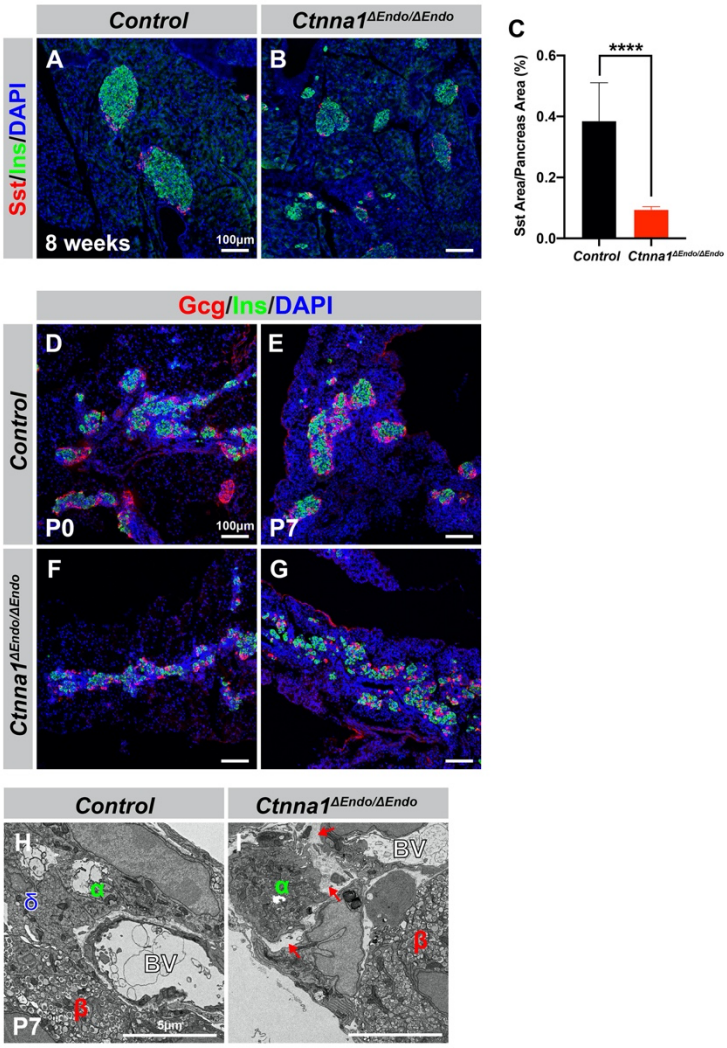

Figure S4. Ctnna1 is required for delta cell survival and normal islet aggregation. Related to Figure 4.

(A-B) Immunofluorescence staining for Sst, Ins, and DAPI in 8 weeks old control and *Ctnna1*$^{\Delta Endo/\Delta Endo}$ pancreas sections. (C) Quantification of Sst^{+} area relative to total pancreas area in 8 weeks old control and *Ctnna1*$^{\Delta Endo/\Delta Endo}$ pancreas sections. (D-G) Immunofluorescence staining for Gcg, Ins, and DAPI in (D,F) P0 and (E,G) P7 control and *Ctnna1*$^{\Delta Endo/\Delta Endo}$ pancreas sections. (H-I) Transmission electron microscope images of P7 (H) control and (I) *Ctnna1*$^{\Delta Endo/\Delta Endo}$ endocrine areas.

Sst, Somatostatin; Ins, Insulin; DAPI, 4',6-diamidino-2-phenylindole; P0, postnatal day 0; P7, postnatal day 7; BV, blood vessels

Data are shown as mean ± SEM. **** $p < 0.0001$.

FIGURE 5

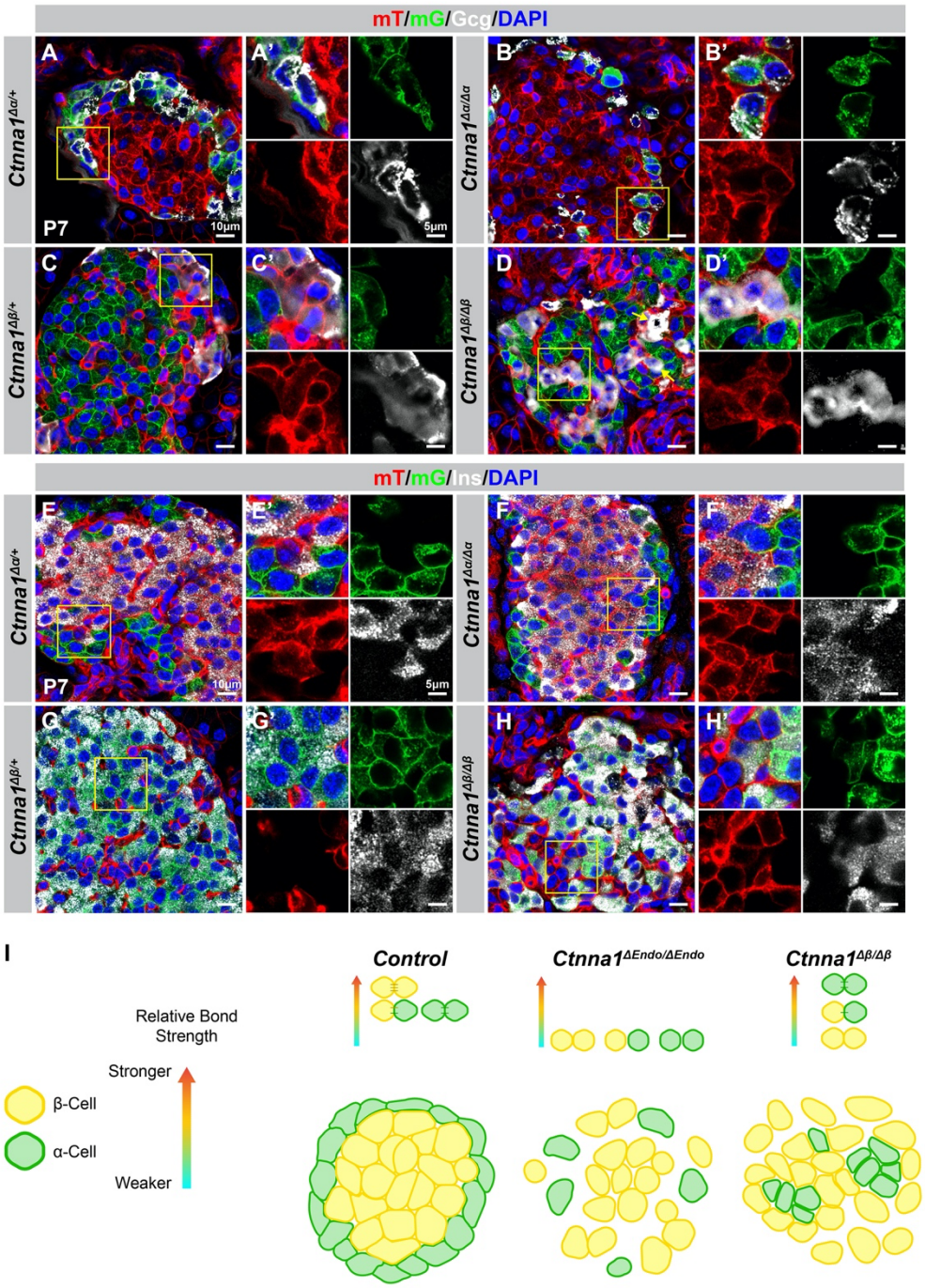
mT/mG/Gcg/DAPI
Ctnna1Δα/+
Ctnna1Δα/Δα
Ctnna1Δβ/+
Ctnna1Δβ/Δβ
A
A'
B
B'
C
C'
D
D'
P7
10μm
5μm
mT/mG/Ins/DAPI
E
E'
F
F'
G
G'
H
H'
I
Control
Ctnna1ΔEndo/ΔEndo
Ctnna1Δβ/Δβ
Relative Bond Strength
Stronger
Weaker
β-Cell
α-Cell

Figure 5. Differential cell-cell adhesion differences between α- and β-cells results in disrupted islet architecture.

(A-H) Airyscan images of immunofluorescence staining of P7 mT/mG reporter mice stained for Gcg, Ins and DAPI in (A,E) heterozygous *Ctnna1*$^{\Delta\alpha/+}$, (B,F) homozygous *Ctnna1*$^{\Delta\alpha/\Delta\alpha}$, (C,G) heterozygous *Ctnna1*$^{\Delta\beta/+}$, and (D,H) homozygous *Ctnna1*$^{\Delta\beta/\Delta\beta}$ mice, showing α-cells entering the islet core (D, yellow allows) in *Ctnna1*$^{\Delta\beta/\Delta\beta}$ mice. Fields demarcated by yellow boxes are shown at higher magnification with individual color channels in side panels. (I) Graphical summary of the differential adhesion hypothesis applied to islet architecture. The α-cells located in the mantle of islets have weaker adhesion than the β-cells located in the islet core. When *Ctnna1* is inactivated in endocrine progenitors, islet architecture is disrupted, and α-cells have weak association with the islet core. When *Ctnna1* is disrupted only in β-cells, α-cells have relatively higher adhesion and are found within the islet core.

Gcg, Glucagon; DAPI, 4',6-diamidino-2-phenylindole; Ins, Insulin; P7, postnatal day 7

SUPPLEMENTARY FIGURE 5: RELATED TO FIGURE 5

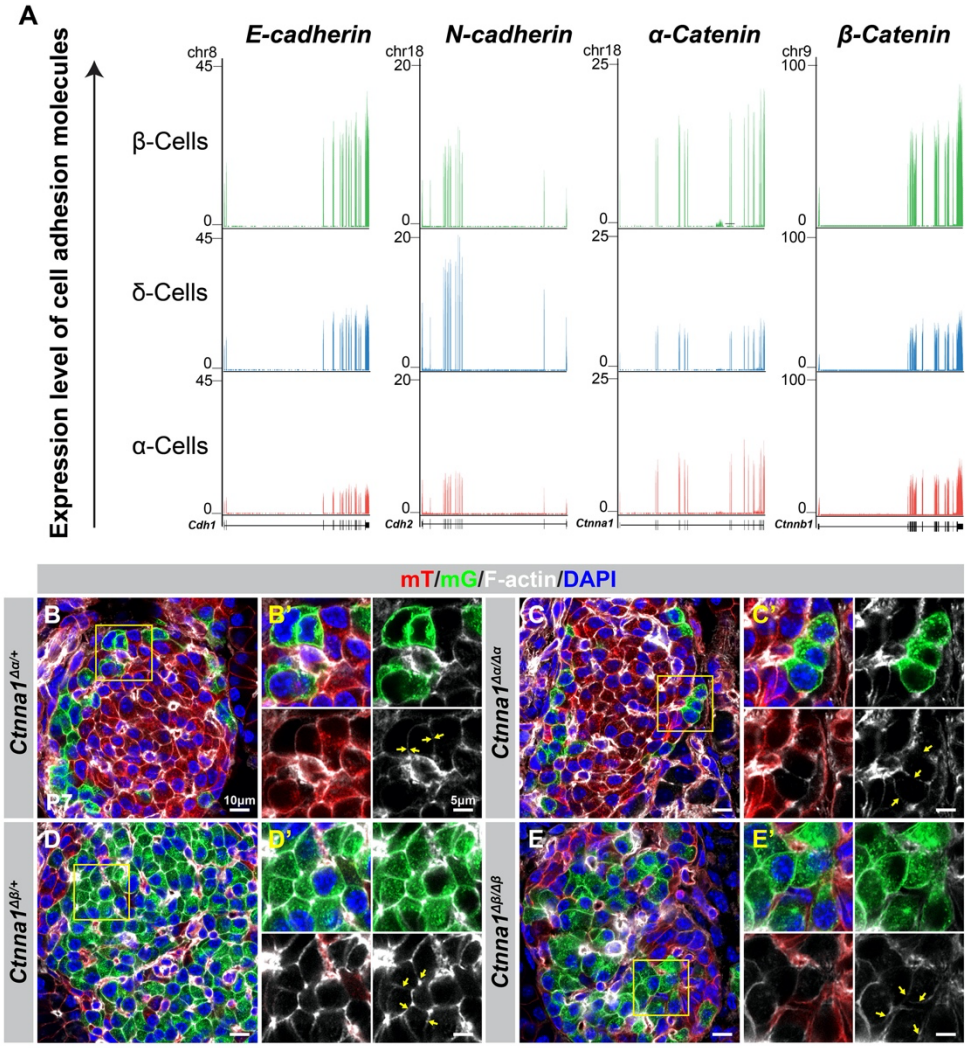

Figure S5. Endocrine cells maintain different cell-cell adhesions. Related to Figure 5.

(A) Genome viewer plots comparing expression levels of adhesion molecules in β-, δ-, and α- cell transcriptomes (DiGruccio et al., 2016). (B-E) Airyscan images of immunofluorescence staining of P7 mT/mG reporter mice stained for F-actin and DAPI in (B) heterozygous *Ctnna1*$^{\Delta\alpha/+}$, (C) homozygous *Ctnna1*$^{\Delta\alpha/\Delta\alpha}$, (D) heterozygous *Ctnna1*$^{\Delta\beta/+}$, and (E) homozygous *Ctnna1*$^{\Delta\beta/\Delta\beta}$ mice. Fields demarcated by yellow boxes in B-E are shown at higher magnification with individual color channels in B'-E' side panels. Yellow arrows indicate expression of F-actin in (B,C) α- and (D,E) β-cells.

DAPI, 4',6-diamidino-2-phenylindole; P7, postnatal day 7

FIGURE 6

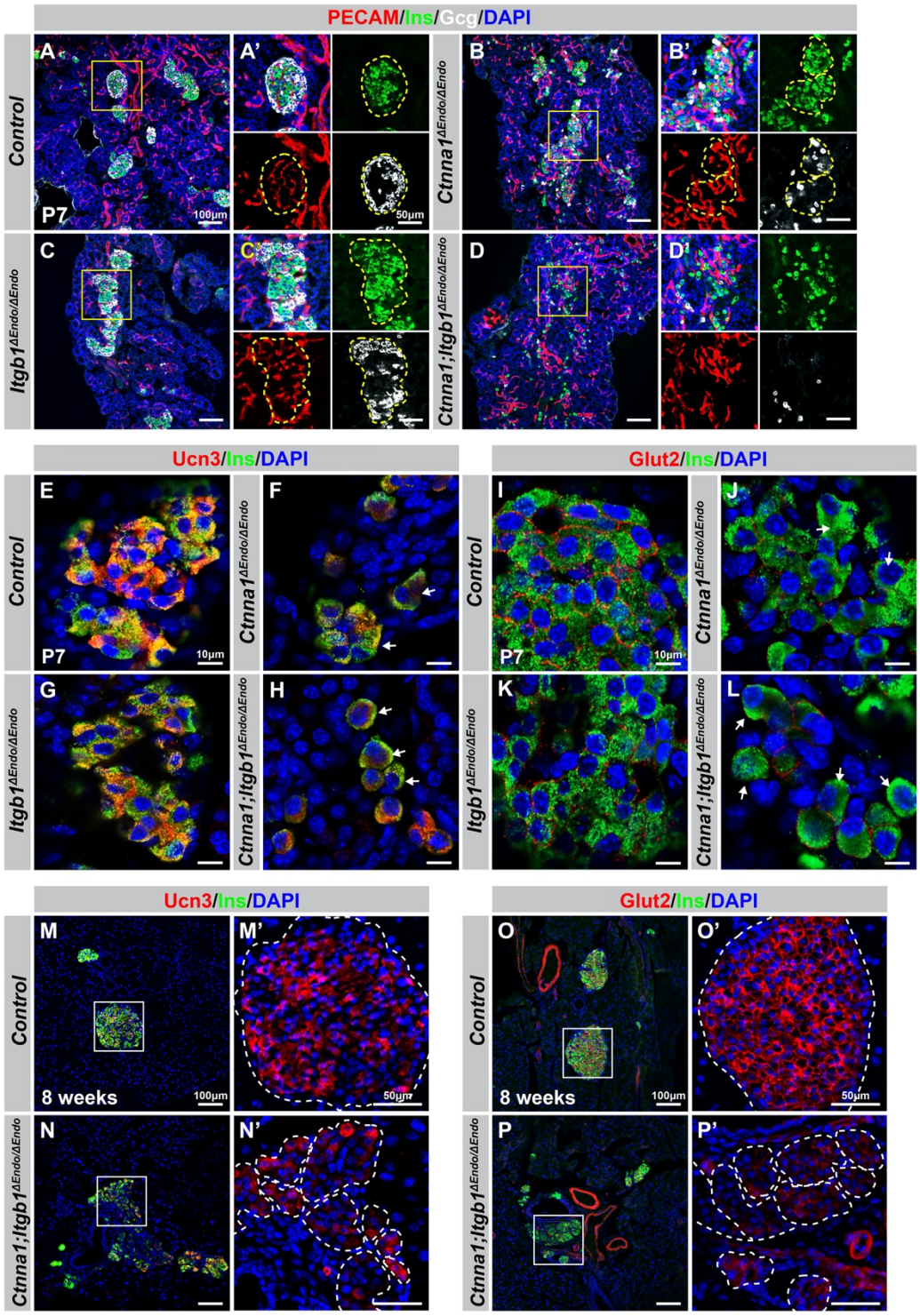
PECAM/Ins/Gcg/DAPI
Control
Ctnna1ΔEndo/ΔEndo
Itgb1ΔEndo/ΔEndo
Ctnna1;Itgb1ΔEndo/ΔEndo
A
A'
B
B'
C
C'
D
D'
P7
100µm
50µm
Ucn3/Ins/DAPI
Glut2/Ins/DAPI
E
F
G
H
I
J
K
L
10µm
M
M'
N
N'
O
O'
P
P'
8 weeks

Figure 6. Disruption of cell-ECM and/or cell-cell adhesion results in abnormal islet vascular architecture, endocrine cell aggregation, and decreased expression of β-cell maturation markers.

(A-D) Immunofluorescence staining of PECAM, Ins, Gcg, and DAPI in P7 (A) control, (B) *Ctnna1*$^{\Delta Endo/\Delta Endo}$, (C) *Itgb1*$^{\Delta Endo/\Delta Endo}$, and (D) *Ctnna1; Itgb1*$^{\Delta Endo/\Delta Endo}$ mice. Fields demarcated by yellow boxes in A-D are shown at higher magnification in A'-D' side panels. Individual islet shape is outlined by dashed yellow lines in A'-D'. Endocrine cells are suspended and scattered throughout the pancreas of *Ctnna1; Itgb1*$^{\Delta Endo/\Delta Endo}$ mice. (E-L) Airyscan images of immunofluorescence staining for Ucn3, Glut2, Ins, and DAPI in P7 (E,I) control, (F,J) *Ctnna1*$^{\Delta Endo/\Delta Endo}$, (G,K) *Itgb1*$^{\Delta Endo/\Delta Endo}$, and (H,L) *Ctnna1; Itgb1*$^{\Delta Endo/\Delta Endo}$ mice. Arrows indicate reduced expression of Ucn3 or Glut2 in β-cells of the mutant mice. (M-P) Immunofluorescence staining of Ucn3, Glut2, Ins, and DAPI in 8 weeks old (M,O) control and (N,P) *Ctnna1; Itgb1*$^{\Delta Endo/\Delta Endo}$ double knockout mice. Fields demarcated by white boxes in M-P are shown at higher magnification in M'-P'. Individual islet shape is outlined by dashed white lines in M'-P'. The reduction of Ucn3 and Glut2 expression persists in adult *Ctnna1; Itgb1*$^{\Delta Endo/\Delta Endo}$ mice.

PECAM, Platelet endothelial cell adhesion molecule-1; Ins, Insulin; Gcg, Glucagon; DAPI, 4',6-diamidino-2-phenylindole; Glut2, Slc2a2; P7, postnatal day 7

SUPPLEMENTARY FIGURE 6: RELATED TO FIGURE 6

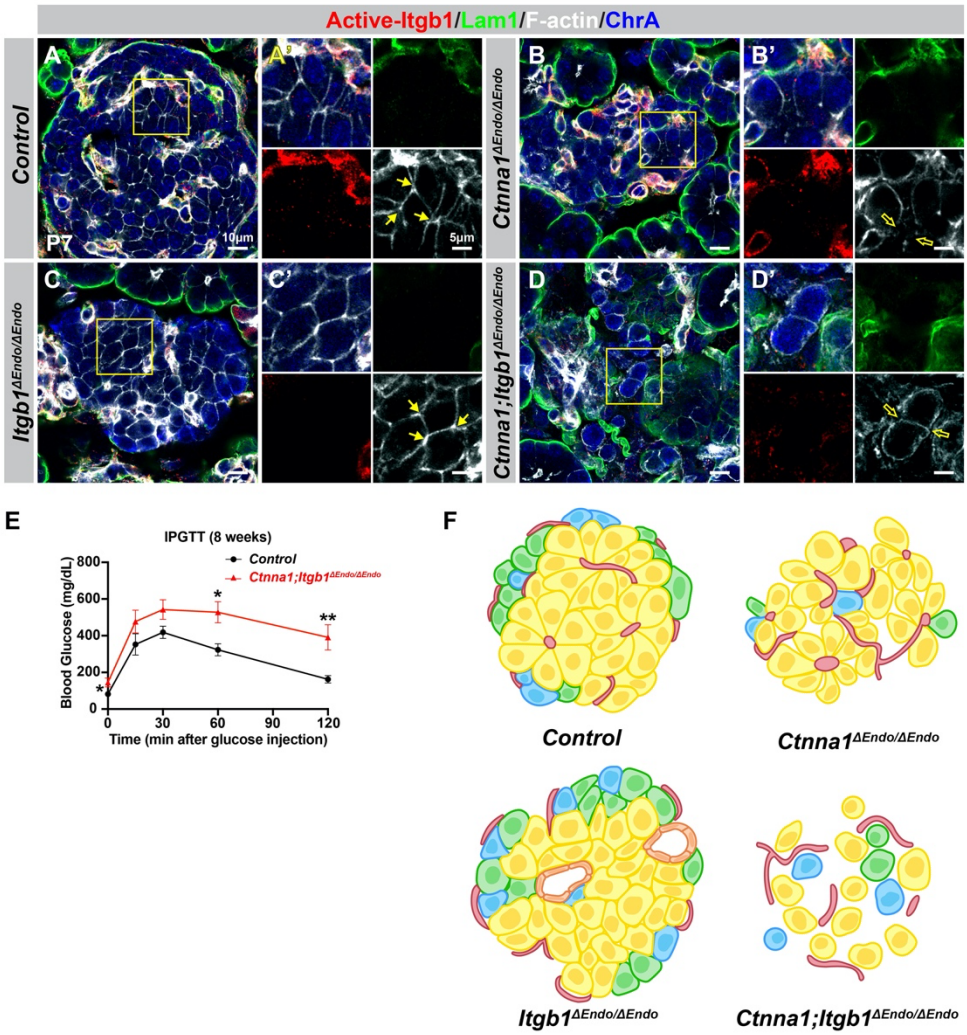

Figure S6. Disruption of cell adhesion results in abnormal endocrine cell aggregation, malformed islet vasculature, and decreased functionality. Related to Figure 6.

(A-D) Airyscan images of immunofluorescence staining for active-Itgb1, Lam1, F-actin and ChrA in (A) control, (B) *Ctnna1*$^{\Delta Endo/\Delta Endo}$, (C) *Itgb1*$^{\Delta Endo/\Delta Endo}$, or (D) *Ctnna1; Itgb1*$^{\Delta Endo/\Delta Endo}$ pancreas sections. Fields demarcated by yellow boxes in A-D are shown at higher magnification in A'-D' side panels. Yellow arrows indicate expression of F-actin in endocrine cells. (E) Intraperitoneal glucose tolerance test on 8 weeks old control and *Ctnna1; Itgb1*$^{\Delta Endo/\Delta Endo}$ mice. (F) Graphical summary of the islet phenotypes observed after disruption of cell-cell and cell-ECM adhesion.

Lam1, Laminin1; ChrA; Chromogranin A; Ins, Insulin; DAPI, 4',6-diamidino-2-phenylindole; P7, postnatal day 7; IPGTT, intraperitoneal glucose tolerance test

Data are shown as mean ± SEM. * $p < 0.05$ and ** $p < 0.01$.

EXPERIMENTAL MODEL AND SUBJECTS DETAILS

Mouse Strains

All animal experiments described herein were approved by the City of Hope Institutional Animal Care and Use Committees. Mice carrying *Ngn3-Cre* (Schonhoff et al., 2004), *R26*$^{mT/mG}$ (Muzumdar et al., 2007), *Gcg-iCre* (Shiota et al., 2017), *Itgb1*^{flox} (Raghavan et al., 2000), *Ctnna1*^{flox} (Vasioukhin et al., 2001), *Ins-Cre* (Thorens et al., 2015), *R26*$^{mT/mG}$ (Muzumdar et al., 2007), *R26*^{EYFP} (Srinivas et al., 2001), and *Ucn3-cre* (Harris et al., 2014) alleles have been previously described. Additional information of the mouse lines used in this study is listed in Supplementary Table 1.

METHOD DETAILS

Whole Mount Immunofluorescence (WMIF)

A standard whole mount staining protocol was utilized to analyze pancreas three-dimensional (3D) morphology, as previously described (Maldonado et al., 2020). Briefly, pancreas tissue, at various embryonic and postnatal stages, was dissected and fixed overnight in 4% paraformaldehyde (PFA). The tissue was dehydrated with serial methanol washes, bleached with a Dent's Bleach solution, and rehydrated using an inverse series of methanol washes. Samples were blocked followed by incubation with primary antibodies for Chromogranin A (ChrA), insulin (Ins), Spp1, and/or PECAM. Samples were then washed in a 0.15% triton-X-PBS solution and stained with secondary antibodies overnight. Following additional washes with 0.15% triton-X-PBS, samples were fixed with 4% PFA, and dehydrated with serial ethanol washes. Finally, samples were immersed in a BABB clearing solution (two parts benzyl benzoate and one part benzyl alcohol) and imaged using a Zeiss LSM880 confocal microscope.

Confocal Microscopy and Image Analysis

All images were collected with a Zeiss LSM880 confocal microscope equipped with a 10X 0.45NA plan apochromat objective at 2X magnification, as standard for AiryScanFast collection. All tiled Z-stacks were acquired in AiryScanFast mode, the acquisition method set to Z-stack (per channel), and with a 2.0 micron step size. Scans were conducted using 405nm, 488nm, 561nm, and 633nm laser lines, and emissions were collected using standard AiryScan filters and the AiryScan detector, in Zen Black 2.3 SP1 (Carl Zeiss). Final voxel sizes were 0.22x0.22x1.98 microns, and

no digital gain or detector offset was used. Detector gains and laser intensities were consistent across all samples.

Image Segmentation/Analysis

Data sets were first AiryScan processed in Zen Black using the “Auto” setting using a 2D sample image as a base for Batch mode. After processing, the files were converted to IMS format and analyzed in Imaris 9.5 (Bitplane). Analysis consisted of manually selecting thresholds that could be consistently applied between samples, and best fit the biology. Due to variations in the depth of the sample, amount of tissue the light had to pass through, and orientation, thresholds were chosen which most accurately represented the objects being analyzed. The ducts were first segmented using a “Surface” with a 2.00-micron surface grain size, and a fixed threshold. We limited the analysis to areas where ducts were present by segmenting the duct channel a second time (again as a Surface) with a grain size of 10 microns and a much lower threshold, generating a “bubble” area of interest around the ducts. Within this volume, endocrine positive staining was then segmented as yet another surface and its distance from the ducts quantified using the median value of the distance transform from the surface of the original ducts. Any endocrine cells contained entirely or mostly within the ducts were considered to have a distance of zero from the ducts.

Immunofluorescence (IF)

Tissues were collected from 6 to 12 weeks old mice and immunofluorescence staining was performed as previously described (Shih et al., 2007). Briefly, pancreata were fixed in 4% paraformaldehyde in PBS, equilibrated in 30% sucrose in PBS, and cryoembedded in Tissue-Tek OCT. Cryoblocks were sectioned at 10 µm intervals. For immunofluorescence staining, sections were blocked for 1 hour prior to the addition of primary antibodies diluted in the same buffer. After washes, secondary antibodies were diluted in blocking buffer and sections were stained for 2 hours at room temperature. Primary and secondary antibodies and their respective dilutions are noted in the Key Resources Table. Apotome images were taken on a Zeiss Axio-Observer-Z1 microscope and figures were created in Adobe Photoshop/Illustrator CC2020. Image-Pro Premier v.9.2 and Qupath software (Free software at https://qupath.github.io) were used to perform morphometric analyses.

Intra Peritoneal Glucose Tolerance Test (IPGTT)

6 to 12 weeks old or 6 to 12 months old mice were fast for 6 hours. Basal blood glucose was measured, and mice were injected intraperitoneally (i.p.) with 2 mg/g body weight dextrose solution. Blood glucose was measured at 15, 30, 45, 60, 90 and 120 minutes after glucose challenge. The experiments were performed by the Comprehensive Metabolic Phenotyping (CMP) Core at City of Hope.

RNA-Sequencing (RNA-seq)

Pancreatic islets were isolated as previously described (Taylor et al., 2013). Total RNA was isolated using the RNeasy Mini Kit (Qiagen) with 10 to 30 isolated islets and processed per manufacturer's instructions. cDNA libraries were prepared using the KAPA RNA HyperPrep Kit with RiboErase (HMR) according to the manufacturer's instructions. Libraries were subjected to high-throughput sequencing on Illumina HiSeq 2500 (50 bp, single-ended) and subsequent data analysis was completed by the Integrative Genomics Core at City of Hope. For sequence alignment and gene counts, RNA-Seq reads were trimmed to remove sequencing adapters using Trimmomatic (Bolger et al., 2014) and polyA tails using FASTP (Chen et al., 2018). The processed reads were mapped back to the mouse genome (mm10) using STAR software (v. 020201) (Dobin et al., 2013). The featureCount software was applied to generate the count matrix, with default parameters (Liao et al., 2019). Between two sets of samples (Wt vs Mut), differential expression analysis was conducted, in R, by adjusting read counts to normalized expression values using TMM normalization method and by correcting batch effects using a design matrix (Robinson et al., 2010). Genes with an FDR-adjusted p-value less than 0.05 and with a fold change (FC) greater than 2 or less than 0.5 were considered as significant up- and down-regulated genes, respectively. Pathway analysis was conducted using DAVID (v. 6.8) (Huang da et al., 2009a, b) and GSEAPreranked algorithm using GSEA Desktop program in Java (Subramanian et al., 2005). The former requires a list of up- and down-regulated genes, while the latter a ranked list of whole genes according to their log2 fold change and p-values. Raw data and processed data files were available at the GEO database:
(GSE153187, https://www.ncbi.nlm.nih.gov/geo/query/acc.cgi?acc=GSE153187).
(GSE190788, https://www.ncbi.nlm.nih.gov/geo/query/acc.cgi?acc=GSE190788).

Ribo-Zero RNA Sequencing Library Preparation and Sequencing

RNA concentration was measured by NanoDrop 1000 (Thermo Fisher Scientific) and RNA integrity was determined using Bioanalyzer (Agilent). Each RNA sample was spiked in with an appropriate amount of either Mix1 or Mix2 according to Life Technologies' guidelines which would

lead to about 1% of the total number of RNA-Seq reads mapping to the 92 ERCC control sequences. The RNA samples were rRNA-depleted and RNAseq libraries were prepared using KAPA RNA HyperPrep Kit with RiboErase (HMR) (Illumina Platforms) (Kapa Biosystems), using 12 cycles of PCR amplification. Libraries were purified using AxyPrep Mag PCR Clean-up kit (Thermo Fisher Scientific). Each library was quantified using a Qubit fluorometer (Life Technologies) and the size distribution assessed using the 2100 Bioanalyzer (Agilent Technologies). Sequencing was performed on an Illumina® NovaSeq 6000 (Illumina) instrument using NovaSeq 6000 Reagent Kit (Illumina®). Quality of sequencing data was checked and combined in one FASTQ file using FastQC v0.11.7

Isolation of mouse pancreatic islets

Mice pancreatic islets were isolated using 2.5 mg/ml collagenase (Sigma Aldrich) as the digestion method. Islets were collected under a stereomicroscope and allowed to recover overnight in PIM(R)® 32A (Prodo Labs) medium with 5% HSA, Gentamicin-AmphotericinB, and 5.8 mmol/L glucose.

Aggregation Assay

Neonatal *Ngn3-Cre; R26mT/mG; Itgb1*$^{+/f}$ (control) *or Ngn3-Cre; R26mT/mG; Itgb1*$^{f/f}$ (mutant) pancreata were dissociated into a single cell suspension using TrypLE (Thermo Fisher). Enzymatic activity was neutralized using FACS buffer (10% fetal bovine serum (FBS) and 2mM EDTA in CMRL media). Cells were passed through a 40 µm cell strainer and DAPI was used to stain dead cells prior to FACS. Prior to cell seeding, 96-well round bottom plates were coated with either bovine serum albumin (BSA; no ECM) or Matrigel and fibronectin (+ECM). 3000 cells per well were added into no ECM or +ECM wells and cultured for 48 hours.

***Ex Vivo* Pancreas Explants**

Pancreas explants are described previously (Shih and Sander, 2014). After 24 hours of culture, the explants were placed on the microscope stage in 37 °C culture chambers with a controlled atmosphere of humidified 5% CO_2. Time-lapse imaging was performed using Zeiss LSM880 inverted confocal microscope with and C-Apochromat 20×/0.75 objective lens. Explants were optically sectioned every 2.5 µm in a 512 × 512 format with up to 80 µm Z-stacks every 10 min for 72 hours. Images were acquired with Zen software and then reconstructed in 3D with in Imaris 9.5 (Bitplane) software. The contrast was adjusted and selected optical planes or *z*-projections of sequential optical sections were used to assemble time-lapse movies.

Electron Microscopy Sample Preparation

Sample blocks were prepared following the NCMIR protocol (T.J. Deerinck, 2010). Briefly, small pieces (1~2 mm^3) of mouse pancreatic tissues were dissected and immediately fixed in 0.2M cacodylate buffer pH7.4 containing 2.5% glutaraldehyde and 2% paraformaldehyde with 3mM calcium chloride. After primary aldehyde fixation the samples were rinsed in 0.15M sodium cacodylate pH7.4 containing 2mM calcium chloride and postfixed in 1.5% potassium ferrocyanide-reduced 2% osmium tetroxide in 0.15M cacodylate buffer for 1 h. Tissue was then rinsed in distilled water and treated with 0.1% aqueous thiocarbohydrazide for 20 min. After further rinsing in distilled water the tissue was again treated with 2% osmium tetroxide for 30 min, rinsed in distilled water, dehydrated in an ethanol series and infiltrated with Durcupan ACM resin. Ultra-thin sections (70 nm thick) were acquired by ultramicrotomy and examined on an FEI Tecnai 12 transmission electron microscope equipped with a Gatan OneView CMOS camera.

Statistics

Statistical analysis was completed using Graphpad Prism. One-way analysis of variance (ANOVA) followed by a student's t-test was utilized to compare groups and represents a minimum of at least three independent measurements. Unless otherwise stated, values are shown as mean ± Standard Error of Mean (SEM).

REFERENCES

1. Adams, M.T., and Blum, B. (2022). Determinants and dynamics of pancreatic islet architecture. Islets *14*, 82-100.
2. Adams, M.T., Dwulet, J.M., Briggs, J.K., Reissaus, C.A., Jin, E., Szulczewski, J.M., Lyman, M.R., Sdao, S.M., Kravets, V., Nimkulrat, S.D.*, et al.* (2021). Reduced synchroneity of intra-islet Ca(2+) oscillations in vivo in Robo-deficient beta cells. Elife *10*.
3. Adams, M.T., Gilbert, J.M., Hinojosa Paiz, J., Bowman, F.M., and Blum, B. (2018). Endocrine cell type sorting and mature architecture in the islets of Langerhans require expression of Roundabout receptors in beta cells. Sci Rep *8*, 10876.
4. Alto, L.T., and Terman, J.R. (2017). Semaphorins and their Signaling Mechanisms. Methods Mol Biol *1493*, 1-25.
5. Arrojo e Drigo, R., Ali, Y., Diez, J., Srinivasan, D.K., Berggren, P.O., and Boehm, B.O. (2015). New insights into the architecture of the islet of Langerhans: a focused cross-species assessment. Diabetologia *58*, 2218-2228.
6. Barros, C.S., Franco, S.J., and Muller, U. (2011). Extracellular matrix: functions in the nervous system. Cold Spring Harb Perspect Biol *3*, a005108.
7. Bastidas-Ponce, A., Tritschler, S., Dony, L., Scheibner, K., Tarquis-Medina, M., Salinno, C., Schirge, S., Burtscher, I., Bottcher, A., Theis, F.J.*, et al.* (2019). Comprehensive single cell mRNA profiling reveals a detailed roadmap for pancreatic endocrinogenesis. Development *146*.
8. Bechard, M.E., Bankaitis, E.D., Hipkens, S.B., Ustione, A., Piston, D.W., Yang, Y.P., Magnuson, M.A., and Wright, C.V. (2016). Precommitment low-level Neurog3 expression defines a long-lived mitotic endocrine-biased progenitor pool that drives production of endocrine-committed cells. Genes Dev *30*, 1852-1865.
9. Bolger, A.M., Lohse, M., and Usadel, B. (2014). Trimmomatic: a flexible trimmer for Illumina sequence data. Bioinformatics *30*, 2114-2120.
10. Campbell, J.E., and Newgard, C.B. (2021). Mechanisms controlling pancreatic islet cell function in insulin secretion. Nat Rev Mol Cell Biol *22*, 142-158.
11. Chen, S., Zhou, Y., Chen, Y., and Gu, J. (2018). fastp: an ultra-fast all-in-one FASTQ preprocessor. Bioinformatics *34*, i884-i890.
12. Cottle, L., Gan, W.J., Gilroy, I., Samra, J.S., Gill, A.J., Loudovaris, T., Thomas, H.E., Hawthorne, W.J., Kebede, M.A., and Thorn, P. (2021). Structural and functional polarisation of human pancreatic beta cells in islets from organ donors with and without type 2 diabetes. Diabetologia *64*, 618-629.

13. Dahl, U., Sjodin, A., and Semb, H. (1996). Cadherins regulate aggregation of pancreatic beta-cells in vivo. Development *122*, 2895-2902.
14. Diaferia, G.R., Jimenez-Caliani, A.J., Ranjitkar, P., Yang, W., Hardiman, G., Rhodes, C.J., Crisa, L., and Cirulli, V. (2013). beta1 integrin is a crucial regulator of pancreatic beta-cell expansion. Development *140*, 3360-3372.
15. DiGruccio, M.R., Mawla, A.M., Donaldson, C.J., Noguchi, G.M., Vaughan, J., Cowing-Zitron, C., van der Meulen, T., and Huising, M.O. (2016). Comprehensive alpha, beta and delta cell transcriptomes reveal that ghrelin selectively activates delta cells and promotes somatostatin release from pancreatic islets. Mol Metab *5*, 449-458.
16. Dobin, A., Davis, C.A., Schlesinger, F., Drenkow, J., Zaleski, C., Jha, S., Batut, P., Chaisson, M., and Gingeras, T.R. (2013). STAR: ultrafast universal RNA-seq aligner. Bioinformatics *29*, 15-21.
17. Dybala, M.P., Butterfield, J.K., Hendren-Santiago, B.K., and Hara, M. (2020). Pancreatic Islets and Gestalt Principles. Diabetes *69*, 1864-1874.
18. Elghazi, L., Gould, A.P., Weiss, A.J., Barker, D.J., Callaghan, J., Opland, D., Myers, M., Cras-Meneur, C., and Bernal-Mizrachi, E. (2012). Importance of beta-Catenin in glucose and energy homeostasis. Sci Rep *2*, 693.
19. Esni, F., Taljedal, I.B., Perl, A.K., Cremer, H., Christofori, G., and Semb, H. (1999). Neural cell adhesion molecule (N-CAM) is required for cell type segregation and normal ultrastructure in pancreatic islets. J Cell Biol *144*, 325-337.
20. Fagotto, F. (2014). The cellular basis of tissue separation. Development *141*, 3303-3318.
21. Foty, R.A., and Steinberg, M.S. (2005). The differential adhesion hypothesis: a direct evaluation. Dev Biol *278*, 255-263.
22. Gilbert, J.M., Adams, M.T., Sharon, N., Jayaraaman, H., and Blum, B. (2020). Morphogenesis of the islets of Langerhans is guided by extra-endocrine Slit2/3 signals. Mol Cell Biol.
23. Gonschior, H., Haucke, V., and Lehmann, M. (2020). Super-Resolution Imaging of Tight and Adherens Junctions: Challenges and Open Questions. Int J Mol Sci *21*.
24. Gouzi, M., Kim, Y.H., Katsumoto, K., Johansson, K., and Grapin-Botton, A. (2011). Neurogenin3 initiates stepwise delamination of differentiating endocrine cells during pancreas development. Dev Dyn *240*, 589-604.
25. Gu, G., Dubauskaite, J., and Melton, D.A. (2002). Direct evidence for the pancreatic lineage: NGN3+ cells are islet progenitors and are distinct from duct progenitors. Development *129*, 2447-2457.

26. Halban, P.A., Powers, S.L., George, K.L., and Bonner-Weir, S. (1987). Spontaneous reassociation of dispersed adult rat pancreatic islet cells into aggregates with three-dimensional architecture typical of native islets. Diabetes *36*, 783-790.
27. Hannigan, G., Troussard, A.A., and Dedhar, S. (2005). Integrin-linked kinase: a cancer therapeutic target unique among its ILK. Nat Rev Cancer *5*, 51-63.
28. Harris, J.A., Hirokawa, K.E., Sorensen, S.A., Gu, H., Mills, M., Ng, L.L., Bohn, P., Mortrud, M., Ouellette, B., Kidney, J.*, et al.* (2014). Anatomical characterization of Cre driver mice for neural circuit mapping and manipulation. Front Neural Circuits *8*, 76.
29. Huang da, W., Sherman, B.T., and Lempicki, R.A. (2009a). Bioinformatics enrichment tools: paths toward the comprehensive functional analysis of large gene lists. Nucleic Acids Res *37*, 1-13.
30. Huang da, W., Sherman, B.T., and Lempicki, R.A. (2009b). Systematic and integrative analysis of large gene lists using DAVID bioinformatics resources. Nat Protoc *4*, 44-57.
31. Jamora, C., and Fuchs, E. (2002). Intercellular adhesion, signalling and the cytoskeleton. Nat Cell Biol *4*, E101-108.
32. Jiang, L., Sun, J., and Huang, D. (2022). Role of Slit/Robo Signaling pathway in Bone Metabolism. Int J Biol Sci *18*, 1303-1312.
33. Jimenez-Caliani, A.J., Pillich, R., Yang, W., Diaferia, G.R., Meda, P., Crisa, L., and Cirulli, V. (2017). alphaE-Catenin Is a Positive Regulator of Pancreatic Islet Cell Lineage Differentiation. Cell Rep *20*, 1295-1306.
34. Jo, J., Kilimnik, G., Kim, A., Guo, C., Periwal, V., and Hara, M. (2011). Formation of pancreatic islets involves coordinated expansion of small islets and fission of large interconnected islet-like structures. Biophys J *101*, 565-574.
35. Kim, A., Miller, K., Jo, J., Kilimnik, G., Wojcik, P., and Hara, M. (2009). Islet architecture: A comparative study. Islets *1*, 129-136.
36. Kragl, M., Schubert, R., Karsjens, H., Otter, S., Bartosinska, B., Jeruschke, K., Weiss, J., Chen, C., Alsteens, D., Kuss, O.*, et al.* (2016). The biomechanical properties of an epithelial tissue determine the location of its vasculature. Nat Commun *7*, 13560.
37. Kwon, H.R., Nelson, D.A., DeSantis, K.A., Morrissey, J.M., and Larsen, M. (2017). Endothelial cell regulation of salivary gland epithelial patterning. Development *144*, 211-220.
38. Lammert, E., Gu, G., McLaughlin, M., Brown, D., Brekken, R., Murtaugh, L.C., Gerber, H.P., Ferrara, N., and Melton, D.A. (2003). Role of VEGF-A in vascularization of pancreatic islets. Curr Biol *13*, 1070-1074.

39. Larsen, H.L., and Grapin-Botton, A. (2017). The molecular and morphogenetic basis of pancreas organogenesis. Semin Cell Dev Biol *66*, 51-68.
40. Lemaire, K., Thorrez, L., and Schuit, F. (2016). Disallowed and Allowed Gene Expression: Two Faces of Mature Islet Beta Cells. Annu Rev Nutr *36*, 45-71.
41. Li, J., Zhao, Z., Wang, J., Chen, G., Yang, J., and Luo, S. (2008). The role of extracellular matrix, integrins, and cytoskeleton in mechanotransduction of centrifugal loading. Mol Cell Biochem *309*, 41-48.
42. Liao, Y., Smyth, G.K., and Shi, W. (2019). The R package Rsubread is easier, faster, cheaper and better for alignment and quantification of RNA sequencing reads. Nucleic Acids Res *47*, e47.
43. Maldonado, M., Serrill, J.D., and Shih, H.P. (2020). Painting the Pancreas in Three Dimensions: Whole-Mount Immunofluorescence Method. Methods Mol Biol *2155*, 193-200.
44. Mohamed, T.H., Watanabe, H., Kaur, R., Belyea, B.C., Walker, P.D., Gomez, R.A., and Sequeira-Lopez, M.L.S. (2020). Renin-Expressing Cells Require beta1-Integrin for Survival and for Development and Maintenance of the Renal Vasculature. Hypertension *76*, 458-467.
45. Mui, K.L., Chen, C.S., and Assoian, R.K. (2016). The mechanical regulation of integrin-cadherin crosstalk organizes cells, signaling and forces. J Cell Sci *129*, 1093-1100.
46. Murtaugh, L.C., Law, A.C., Dor, Y., and Melton, D.A. (2005). Beta-catenin is essential for pancreatic acinar but not islet development. Development *132*, 4663-4674.
47. Muzumdar, M.D., Tasic, B., Miyamichi, K., Li, L., and Luo, L. (2007). A global double-fluorescent Cre reporter mouse. Genesis *45*, 593-605.
48. Nair, G.G., Liu, J.S., Russ, H.A., Tran, S., Saxton, M.S., Chen, R., Juang, C., Li, M.L., Nguyen, V.Q., Giacometti, S.*, et al.* (2019). Recapitulating endocrine cell clustering in culture promotes maturation of human stem-cell-derived beta cells. Nat Cell Biol *21*, 263-274.
49. Panzer, J.K., Cohrs, C.M., and Speier, S. (2020). Using Pancreas Tissue Slices for the Study of Islet Physiology. Methods Mol Biol *2128*, 301-312.
50. Pauerstein, P.T., Tellez, K., Willmarth, K.B., Park, K.M., Hsueh, B., Efsun Arda, H., Gu, X., Aghajanian, H., Deisseroth, K., Epstein, J.A.*, et al.* (2017). A radial axis defined by semaphorin-to-neuropilin signaling controls pancreatic islet morphogenesis. Development *144*, 3744-3754.

51. Raghavan, S., Bauer, C., Mundschau, G., Li, Q., and Fuchs, E. (2000). Conditional ablation of beta1 integrin in skin. Severe defects in epidermal proliferation, basement membrane formation, and hair follicle invagination. J Cell Biol *150*, 1149-1160.
52. Reinert, R.B., Cai, Q., Hong, J.Y., Plank, J.L., Aamodt, K., Prasad, N., Aramandla, R., Dai, C., Levy, S.E., Pozzi, A.*, et al.* (2014). Vascular endothelial growth factor coordinates islet innervation via vascular scaffolding. Development *141*, 1480-1491.
53. Robinson, M.D., McCarthy, D.J., and Smyth, G.K. (2010). edgeR: a Bioconductor package for differential expression analysis of digital gene expression data. Bioinformatics *26*, 139-140.
54. Romer, A.I., and Sussel, L. (2015). Pancreatic islet cell development and regeneration. Curr Opin Endocrinol Diabetes Obes *22*, 255-264.
55. Roscioni, S.S., Migliorini, A., Gegg, M., and Lickert, H. (2016). Impact of islet architecture on beta-cell heterogeneity, plasticity and function. Nat Rev Endocrinol *12*, 695-709.
56. Rosenberg, L.C., Lafon, M.L., Pedersen, J.K., Yassin, H., Jensen, J.N., Serup, P., and Hecksher-Sorensen, J. (2010). The transcriptional activity of Neurog3 affects migration and differentiation of ectopic endocrine cells in chicken endoderm. Dev Dyn *239*, 1950-1966.
57. Rulifson, I.C., Karnik, S.K., Heiser, P.W., ten Berge, D., Chen, H., Gu, X., Taketo, M.M., Nusse, R., Hebrok, M., and Kim, S.K. (2007). Wnt signaling regulates pancreatic beta cell proliferation. Proc Natl Acad Sci U S A *104*, 6247-6252.
58. Sakai, T., Larsen, M., and Yamada, K.M. (2003). Fibronectin requirement in branching morphogenesis. Nature *423*, 876-881.
59. Scheppke, L., Murphy, E.A., Zarpellon, A., Hofmann, J.J., Merkulova, A., Shields, D.J., Weis, S.M., Byzova, T.V., Ruggeri, Z.M., Iruela-Arispe, M.L.*, et al.* (2012). Notch promotes vascular maturation by inducing integrin-mediated smooth muscle cell adhesion to the endothelial basement membrane. Blood *119*, 2149-2158.
60. Schonhoff, S.E., Giel-Moloney, M., and Leiter, A.B. (2004). Neurogenin 3-expressing progenitor cells in the gastrointestinal tract differentiate into both endocrine and non-endocrine cell types. Dev Biol *270*, 443-454.
61. Scully, K.M., Skowronska-Krawczyk, D., Krawczyk, M., Merkurjev, D., Taylor, H., Livolsi, A., Tollkuhn, J., Stan, R.V., and Rosenfeld, M.G. (2016). Epithelial cell integrin beta1 is required for developmental angiogenesis in the pituitary gland. Proc Natl Acad Sci U S A *113*, 13408-13413.

62. Seymour, P.A., Bennett, W.R., and Slack, J.M. (2004). Fission of pancreatic islets during postnatal growth of the mouse. J Anat *204*, 103-116.
63. Sharon, N., Chawla, R., Mueller, J., Vanderhooft, J., Whitehorn, L.J., Rosenthal, B., Gurtler, M., Estanboulieh, R.R., Shvartsman, D., Gifford, D.K.*, et al.* (2019a). A Peninsular Structure Coordinates Asynchronous Differentiation with Morphogenesis to Generate Pancreatic Islets. Cell *176*, 790-804 e713.
64. Sharon, N., Vanderhooft, J., Straubhaar, J., Mueller, J., Chawla, R., Zhou, Q., Engquist, E.N., Trapnell, C., Gifford, D.K., and Melton, D.A. (2019b). Wnt Signaling Separates the Progenitor and Endocrine Compartments during Pancreas Development. Cell Rep *27*, 2281-2291 e2285.
65. Shih, H.P., Gross, M.K., and Kioussi, C. (2007). Cranial muscle defects of Pitx2 mutants result from specification defects in the first branchial arch. Proc Natl Acad Sci U S A *104*, 5907-5912.
66. Shih, H.P., Panlasigui, D., Cirulli, V., and Sander, M. (2016). ECM Signaling Regulates Collective Cellular Dynamics to Control Pancreas Branching Morphogenesis. Cell Rep *14*, 169-179.
67. Shih, H.P., and Sander, M. (2014). Pancreas development ex vivo: culturing embryonic pancreas explants on permeable culture inserts, with fibronectin-coated glass microwells, or embedded in three-dimensional Matrigel. Methods Mol Biol *1210*, 229-237.
68. Shih, H.P., Wang, A., and Sander, M. (2013). Pancreas organogenesis: from lineage determination to morphogenesis. Annu Rev Cell Dev Biol *29*, 81-105.
69. Shiota, C., Prasadan, K., Guo, P., Fusco, J., Xiao, X., and Gittes, G.K. (2017). Gcg (CreERT2) knockin mice as a tool for genetic manipulation in pancreatic alpha cells. Diabetologia *60*, 2399-2408.
70. Srinivas, S., Watanabe, T., Lin, C.S., William, C.M., Tanabe, Y., Jessell, T.M., and Costantini, F. (2001). Cre reporter strains produced by targeted insertion of EYFP and ECFP into the ROSA26 locus. BMC Dev Biol *1*, 4.
71. Stine, R.R., Greenspan, L.J., Ramachandran, K.V., and Matunis, E.L. (2014). Coordinate regulation of stem cell competition by Slit-Robo and JAK-STAT signaling in the Drosophila testis. PLoS Genet *10*, e1004713.
72. Subramanian, A., Tamayo, P., Mootha, V.K., Mukherjee, S., Ebert, B.L., Gillette, M.A., Paulovich, A., Pomeroy, S.L., Golub, T.R., Lander, E.S.*, et al.* (2005). Gene set enrichment analysis: a knowledge-based approach for interpreting genome-wide expression profiles. Proc Natl Acad Sci U S A *102*, 15545-15550.

73. Sznurkowska, M.K., Hannezo, E., Azzarelli, R., Chatzeli, L., Ikeda, T., Yoshida, S., Philpott, A., and Simons, B.D. (2020). Tracing the cellular basis of islet specification in mouse pancreas. Nat Commun *11*, 5037.
74. T.J. Deerinck, E.B., A. Thor, M.H. Ellisman (2010). NCMIR Methods for 3D EM: A New Protocol for Preparation of Biological Specimens for Serial Block Face Scanning Electron Microscopy. In National Center for Microscopy and Imaging Research, University of California, San Diego
75. Taylor, B.L., Liu, F.F., and Sander, M. (2013). Nkx6.1 is essential for maintaining the functional state of pancreatic beta cells. Cell Rep *4*, 1262-1275.
76. Thorens, B., Tarussio, D., Maestro, M.A., Rovira, M., Heikkila, E., and Ferrer, J. (2015). Ins1(Cre) knock-in mice for beta cell-specific gene recombination. Diabetologia *58*, 558-565.
77. Tong, M., Jun, T., Nie, Y., Hao, J., and Fan, D. (2019). The Role of the Slit/Robo Signaling Pathway. J Cancer *10*, 2694-2705.
78. Vasioukhin, V., Bauer, C., Degenstein, L., Wise, B., and Fuchs, E. (2001). Hyperproliferation and defects in epithelial polarity upon conditional ablation of alpha-catenin in skin. Cell *104*, 605-617.
79. Wakae-Takada, N., Xuan, S., Watanabe, K., Meda, P., and Leibel, R.L. (2013). Molecular basis for the regulation of islet beta cell mass in mice: the role of E-cadherin. Diabetologia *56*, 856-866.
80. Wang, S., Matsumoto, K., Lish, S.R., Cartagena-Rivera, A.X., and Yamada, K.M. (2021). Budding epithelial morphogenesis driven by cell-matrix versus cell-cell adhesion. Cell *184*, 3702-3716 e3730.
81. Wang, S., Sekiguchi, R., Daley, W.P., and Yamada, K.M. (2017). Patterned cell and matrix dynamics in branching morphogenesis. J Cell Biol *216*, 559-570.
82. Weber, G.F., Bjerke, M.A., and DeSimone, D.W. (2011). Integrins and cadherins join forces to form adhesive networks. J Cell Sci *124*, 1183-1193.
83. Win, P.W., Oakie, A., Li, J., and Wang, R. (2020). Beta-cell beta1 integrin deficiency affects in utero development of islet growth and vascularization. Cell Tissue Res *381*, 163-175.
84. Yamamoto, H., Ehling, M., Kato, K., Kanai, K., van Lessen, M., Frye, M., Zeuschner, D., Nakayama, M., Vestweber, D., and Adams, R.H. (2015). Integrin beta1 controls VE-cadherin localization and blood vessel stability. Nat Commun *6*, 6429.